Journal of Materials Chemistry A

REVIEW

View Article Online
View Journal

Cite this: DOI: 10.1039/d5ta04044b

Architecting light for catalysis: emerging frontiers in plasmonic–photonic crystal hybrids for solar energy conversion

Tharishinny Raja Mogan*[a] and Hiang Kwee Lee *[ab]

Plasmonic–photonic crystal (PPC) photocatalysts have emerged as a promising class of materials that integrate nanoscale light management with catalytic functionality for solar-driven chemical conversions. By combining the electromagnetic field enhancement of plasmonic nanostructures with the photon manipulation capabilities of photonic crystals, PPCs effectively address key limitations of traditional semiconductor photocatalysts, including limited visible light absorption and rapid charge recombination. This review provides a comprehensive overview of recent advances in PPCs. It outlines the fundamental physical principles of plasmonics, photonic bandgap effects, and their synergistic interactions in hybrid systems. A range of fabrication strategies, from bottom–up self-assembly to top–down lithography, is presented with an emphasis on achieving structural precision and spectral alignment. The discussion also covers advanced design concepts such as hierarchical architectures, multifunctional plasmonic catalysts, and dynamically tunable photonic structures. These innovations have drastically improved photocatalytic performance under visible light, particularly in applications involving total water splitting, hydrogen evolution reaction, and carbon dioxide reduction. In addition, this review critically examines ongoing challenges, including achieving long-term stability, developing scalable fabrication techniques, and enhancing the utilization of light and photogenerated charge carriers. It concludes by proposing future research directions, ranging from the exploration of earth-abundant plasmonic materials to the integration of PPCs into functional device architectures. Overall, plasmonic–photonic crystals offer a transformative strategy for solar fuel production by enabling precise control over light–matter interactions, and this review aims to support the rational design of next-generation hybrid photocatalysts for efficient and sustainable energy applications.

Received 20th May 2025
Accepted 29th July 2025

DOI: 10.1039/d5ta04044b

rsc.li/materials-a

[a]Division of Chemistry and Biological Chemistry, School of Chemistry, Chemical Engineering and Biotechnology, Nanyang Technological University, 21 Nanyang Link, Singapore 637371, Singapore. E-mail: tharishinny.rm@ntu.edu.sg; hiangkwee@ntu.edu.sg

[b]Institute of Materials Research and Engineering, The Agency for Science, Technology and Research (A*STAR), 2 Fusionopolis Way, #08-03, Innovis, 138634, Singapore

Tharishinny Raja Mogan

Tharishinny Raja Mogan is a Research Fellow at the School of Chemistry, Chemical Engineering and Biotechnology, Nanyang Technological University. She completed her PhD in Materials Science at Hokkaido University, Japan in 2021. Her research focuses on photonic crystal-based hybrids for enhanced light–matter interactions in optical and catalytic applications.

Hiang Kwee Lee

Hiang Kwee Lee is a Nanyang Assistant Professor at the School of Chemistry, Chemical Engineering and Biotechnology at Nanyang Technological University. He earned both his PhD and bachelor's degrees in Chemistry from Nanyang Technological University in 2018 and 2013, respectively. His research program combines chemistry, nanotechnology, materials science, and in operando spectroscopy to develop next-generation catalytic ensembles aimed at addressing global energy and environmental crises.

1. Introduction

Photocatalysis, wherein light energy activates a catalyst to accelerate chemical transformations, has emerged as a promising approach to address global challenges in energy conversion and environmental remediation.[1,2] In solar photocatalysis, abundant sunlight is harnessed to drive reactions that produce clean fuels (*e.g.* hydrogen and ammonia) or degrade pollutants, offering routes to sustainable energy and water purification.[3–6] An ideal photocatalyst efficiently absorbs a broad spectrum of sunlight and converts photons into chemical energy. However, conventional semiconductor photocatalysts face two major limitations. First, light harvesting is often poor as many widely studied semiconductors (*e.g.*, TiO_2 and ZnO) have large band gaps (~3.0–3.2 eV for anatase TiO_2) and thus only absorb UV light, which accounts for a mere ~5% of the solar spectrum.[7–9] Visible light passes through unused, severely limiting solar energy utilization. Second, rapid charge recombination remains a critical limitation, as photoexcited electrons and holes often recombine before participating in surface redox reactions, thereby reducing photocatalytic efficiency.[10,11] These issues result in low quantum efficiencies and pose a need for innovative strategies to boost light absorption and charge separation in photocatalytic materials.

Over the years, researchers have developed various methods to improve the performance of semiconductor-based photocatalysts under solar illumination. Bandgap engineering (*e.g.*, doping with metal or non-metal ions) can extend absorption into the visible range, but this often introduces mid-gap states that act as recombination centers, which diminish photocarrier utilization efficiency.[12–15] Sensitization with dyes or quantum dots can broaden absorption, but it suffers from poor intrinsic photostability.[16,17] A particularly effective approach has been loading noble metal nanoparticles onto semiconductor surfaces, creating plasmonic photocatalysts.[18–20] Noble metals such as Au and Ag exhibit strong localized surface plasmon resonance (LSPR) in the visible range. These plasmonic nanoparticles further act as visible-light antennas and electron traps when coupled with a semiconductor.[21,22] Early studies by Bard and others in the 1980s showed that depositing noble metals on TiO_2 can enhance UV photocatalysis by scavenging electrons.[23] These plasmonic photocatalysts leverage the unique optical and electronic effects of metal nanoparticles, including intense electromagnetic near fields, hot electron generation, and photothermal conversion to enhance solar-driven reaction rates.[24–26] Indeed, a flurry of reports in the past decade has demonstrated improved photocurrent generation, pollutant degradation, H_2 production, and CO_2 reduction under visible light by incorporating Au or Ag onto semiconductors.[27–30] However, even with plasmonic enhancement, a large portion of incident light may still go unabsorbed or not effectively converted.

To better utilize the incident light, photonic crystals (PCs) have emerged as promising light-manipulating architectures capable for enhancing photocatalytic performance.[31–33] Notably, PCs are characterized by their unique structural features comprising periodically ordered dielectric structures on the scale of optical wavelengths, which correspondingly facilitates light–matter interactions. By introducing a periodic modulation in the refractive index, PCs create photonic bandgaps (also known as stop bands) that forbid certain wavelengths from propagating.[34,35] At the blue edge and red edge of these photonic bandgaps, incident light experiences slow photon effects as the group velocity of photons is greatly reduced, leading to enhanced local electromagnetic field intensity and prolonged light–matter interaction.[36,37] In essence, PCs can trap or recycle light within a photocatalyst, increasing the path length and probability of light absorption.[38–40] Researchers have integrated TiO_2 into PC architectures such as in inverse opals with three-dimensional (3D) periodic porosity or in one-dimensional (1D) Bragg stacks. These TiO_2-based PCs have been demonstrated to enhance light harvesting and photocatalytic activity attributed to slow-photon effects at the photonic band edge and multiple light-scattering phenomena within the periodic dielectric frameworks.[31,33,41,42] Such precise structuring of optical materials addresses the light absorption challenge from a physical perspective, thereby complementing the chemical approaches of doping or sensitization.

More interestingly, combining plasmonic and photonic strategies has led to the emerging concept of plasmonic photonic crystals as hybrid photocatalysts that integrate metal nanostructures with PC architectures for synergistic light utilization.[43–47] The rationale is compelling as PCs can trap incoming light and concentrate it within specific spectral regions, while the plasmonic nanoparticles strongly absorb that light to generate intense localized electromagnetic fields which, upon plasmon decay, produce energetic charge carriers that drive redox reaction. If designed properly, the photonic bandgap can be tuned to overlap with the LSPR frequency of the metal nanoparticles, enabling plasmon resonance enhancement *via* slow photons within the PC. This mutual enhancement can dramatically amplify the local electromagnetic field and boost the rate of useful photochemical reactions. For instance, initial studies have indeed shown large gains in performance when aligning photonic and plasmonic effects. For example, Zhang *et al.*[48] demonstrated that assembling 20 nm Au nanocrystals (LSPR peak ~556 nm) onto a TiO_2 inverse opal photonic crystal drastically increased hot electron injection and achieved one of the highest visible-light water-splitting photocurrents reported for Au/TiO_2 systems. Likewise, recent reports indicate that matching the LSPR of Au or Ag with the photonic stop band edge of a TiO_2 photonic crystal can more than double the photocatalytic reaction rates compared to non-structured catalysts.[44,45] On the other hand, poor alignment of plasmonic and photonic features can be counterproductive. When the plasmon absorbs in a spectral range not enhanced by the PC, the photocatalytic benefit may be negligible or even diminished.[46] Thus, rational design is key to harnessing the full potential of plasmonic PCs. Given the growing body of promising studies, a comprehensive review is needed to consolidate recent progress, clarify underlying mechanisms, and provide design guidelines that can accelerate the development of plasmonic–photonic crystals for high-efficiency solar energy photocatalysis.

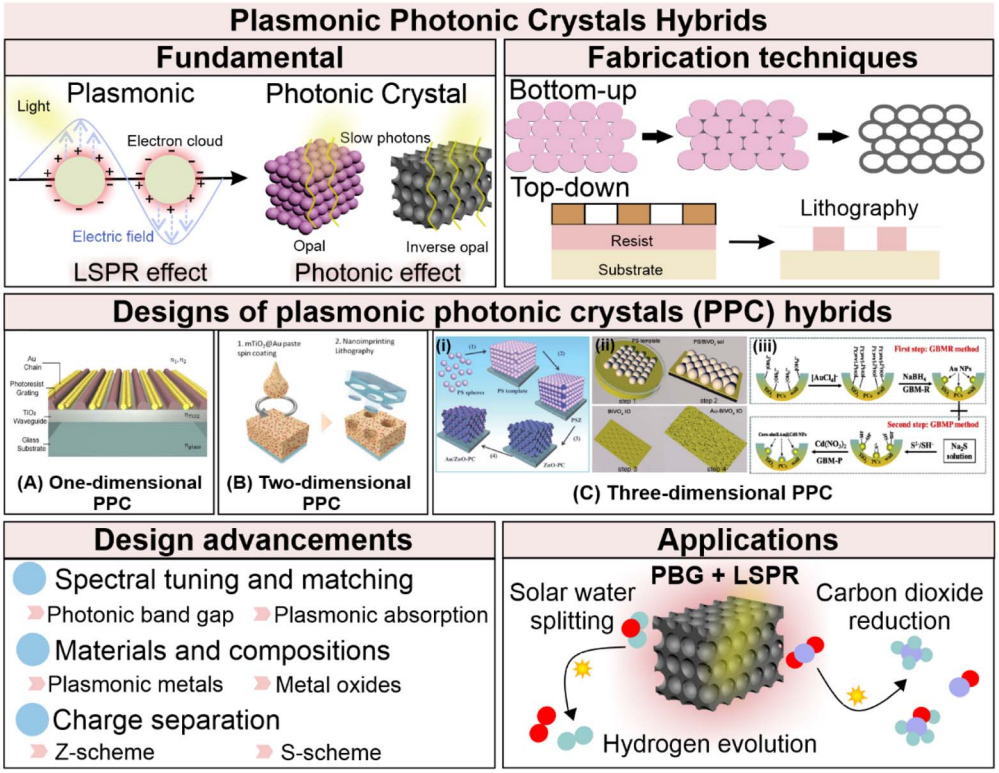

Fig. 1 Overview of plasmonic–photonic crystal (PPC) photocatalysts, from fundamentals to energy applications. (A) Schematic illustration of one-dimensional PPC hybrids, where plasmonic nanoparticle gratings are self-assembled within a photoresist template on a TiO_2 waveguide. Reproduced with permission from ref. 49. Copyright 2019 American Chemical Society. (B) Schematic illustration of two-dimensional PPC hybrids based on a fabrication scheme involving nanostructured photocatalytic substrates integrated with *ex situ* grown Au nanoparticles. Reproduced with permission from ref. 50. Copyright 2021 Wiley. (C) Schematic illustration of three-dimensional PPC hybrids. (i) Au/ZnO photonic crystal hybrids fabricated *via* four steps: (1) self-assembly of polystyrene (PS) spheres into a face-centered cubic structure, (2) infiltration with a ZnO precursor, (3) drying and calcination, and (4) sputtering of Au nanoparticles onto the ZnO-PC. Reproduced with permission from ref. 51. Copyright 2015 Royal Society of Chemistry. (ii) Au nanocrystal-decorated $BiVO_4$ inverse opal (IO) fabricated through (1) monolayer PS sphere self-assembly at the $BiVO_4$ sol–air interface, (2) transfer onto ITO glass, (3) annealing to form $BiVO_4$ IO, and (4) thermal evaporation of Au nanocrystals. Reproduced with permission from ref. 52. Copyright 2021 Royal Society of Chemistry. (iii) Au@CdS core–shell nanoparticles supported on an inverse opal TiO_2 scaffold, synthesized *via* a two-step gas bubbling-assisted membrane reduction–precipitation (GBMR/P) method. Reproduced with permission from ref. 53. Copyright 2015 Elsevier.

Herein, this review presents a detailed examination of plasmonic–photonic crystal photocatalysts, with a focus on recent breakthroughs and emerging design principles (Fig. 1). We first cover the fundamental theoretical background of plasmonics, PCs, and their hybrid interactions (Section 2). We then discuss fabrication techniques (Section 3) for creating these complex nanostructures, ranging from bottom–up self-assembly to top–down nanolithography. In Section 4, we highlight design advancements aimed at enhancing light–matter interactions and charge separation, including novel architectures and material combinations. Section 5 focuses on applications in energy-related photocatalysis, including solar water splitting, CO_2 reduction, and H_2 generation, where these plasmonic–photonic platforms have shown notable performance improvements. Finally, Section 6 provides a forward-looking perspective, outlining the key challenges that remain and highlighting future research directions to advance this dynamic and interdisciplinary field. By integrating insights from recent high-impact studies, we aim to convey both the current state and the future promise of plasmonic PCs as next-generation photocatalysts for efficient solar fuel production.

2. Theoretical background

2.1. Plasmonics and photocatalysis fundamentals

Plasmonics centers on the behavior of conduction electrons in metal nanostructures under oscillating electromagnetic fields. When light of appropriate frequency strikes a noble metal nanometer-sized particle, the free electrons collectively oscillate in resonance with the incident field, resulting in a phenomenon known as LSPR (Fig. 2A).[54] This resonant oscillation leads to extremely strong electromagnetic fields localized near the nanoparticle's surface (often orders of magnitude stronger than the incident field). For gold (Au) and silver (Ag) nanoparticles, LSPR typically occurs in the visible to near-infrared range (*e.g.* ~520 nm for 20 nm Au spheres and ~400 nm for Ag spheres), and the exact wavelength can be tuned by varying particle size, shape (nanosphere, nanocubes, nanorods, and nanobranches),

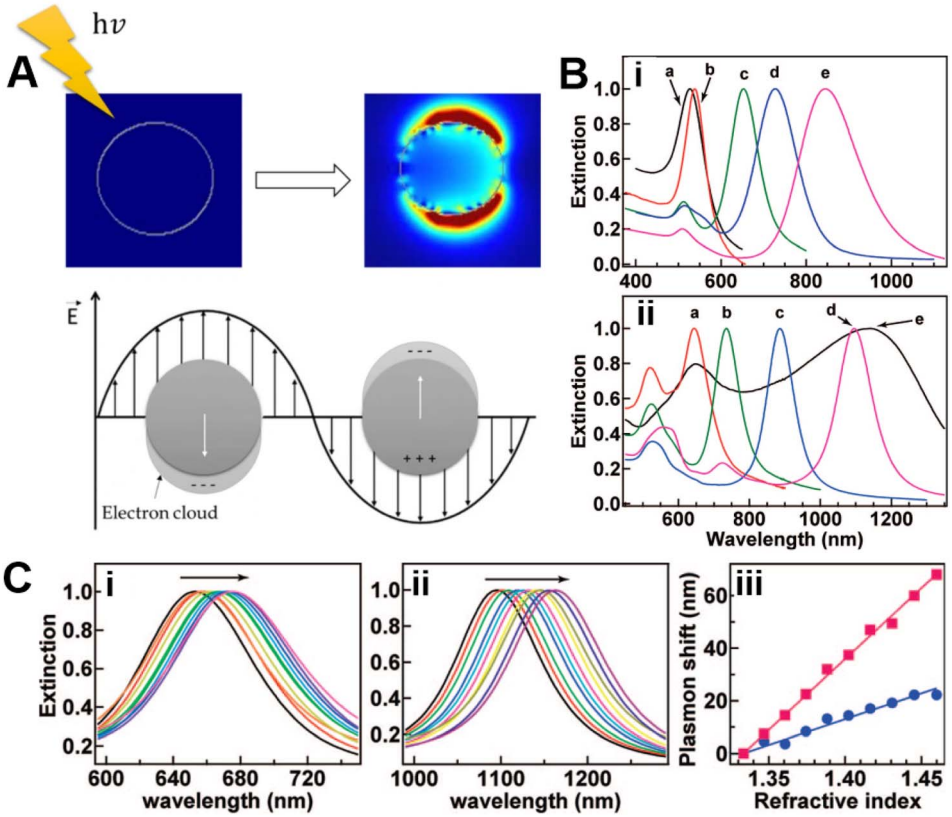

Fig. 2 (A) Schematic illustration of LSPR in metal nanoparticles induced by incident light waves. Reproduced with permission from ref. 54. Copyright 2023 Springer Nature. (B) Normalized extinction spectra of Au nanoparticles with different shapes and sizes. (i) Spectra a–e correspond to nanospheres, nanocubes, and nanorods with different aspect ratios, respectively. (ii) Spectra a–e correspond to nanobipyramids with increasing aspect ratios and nanobranches, respectively. (C) (i) Extinction spectra of Au nanorods dispersed in water–glycerol mixtures with varying compositions. (ii) Extinction spectra of Au nanobipyramids water–glycerol mixtures with varying compositions. Arrows indicate the direction of increasing glycerol volume percentage. (iii) Longitudinal plasmon resonance shift as a function of the refractive index of the liquid mixtures, for the Au nanorods (blue circles) and nanobipyramids (red squares) shown in (i) and (ii), respectively. Reproduced with permission from ref. 59. Copyright 2008 American Chemical Society.

composition, and the surrounding medium's refractive index (Fig. 2B and C).[55–59]

LSPR plays a vital role in photocatalysis through two primary mechanisms. First, the enhanced local electromagnetic fields generated near plasmonic nanostructures can drastically increase light absorption in adjacent semiconductors or molecules (Fig. 3A). By functioning as a nanoscale antenna, these intensified fields concentrate incident light into the active material, thereby boosting photocatalytic efficiency.[60,61] Second, when the plasmon decays either through radiative scattering or nonradiative damping, it releases energy that can generate energetic charge carriers (hot electrons and holes) within the metal or elevate the local temperature.[62,63]

In plasmonic photocatalysts comprising of metal–semiconductor hybrids, three primary enhancement mechanisms are widely recognized. First, hot electron injection occurs when the excitation of LSPR in metal nanoparticles generates energetic electrons that can be transferred into the conduction band of a neighbouring semiconductor (Fig. 3B). These electrons can drive surface redox reactions, thereby extending the light absorption capabilities of wide bandgap semiconductors into the visible range. In this role, the metal acts as a plasmonic sensitizer, functioning similarly to a photosensitizing dye.[64] Second, plasmon-induced energy transfer enables direct excitation of electrons in the semiconductor through energy transfer from the metal nanoparticle. This mechanism is analogous to Förster resonance energy transfer and becomes particularly effective when the LSPR energy matches an optical transition in the semiconductor, especially where the absorption edge overlaps with the plasmon resonance.[65] Third, photothermal effects resulting from nonradiative plasmon decay lead to localized heating at the catalyst–adsorbate interface, which in turn accelerates reaction kinetics by increasing the local temperature (Fig. 3C and D).[66] Collectively, these mechanisms illustrate the multifaceted ways in which plasmonic structures can enhance photocatalytic performance.

In many systems, these mechanisms can occur simultaneously. For instance, under visible light irradiation, a Au–TiO_2 photocatalyst may inject hot electrons into the TiO_2 conduction band while also increasing the local temperature, both of which contribute to improved catalytic performance.[67] The relative contribution of each pathway varies depending on the specific system and experimental conditions. Ongoing research employs advanced spectroscopic techniques such as transient

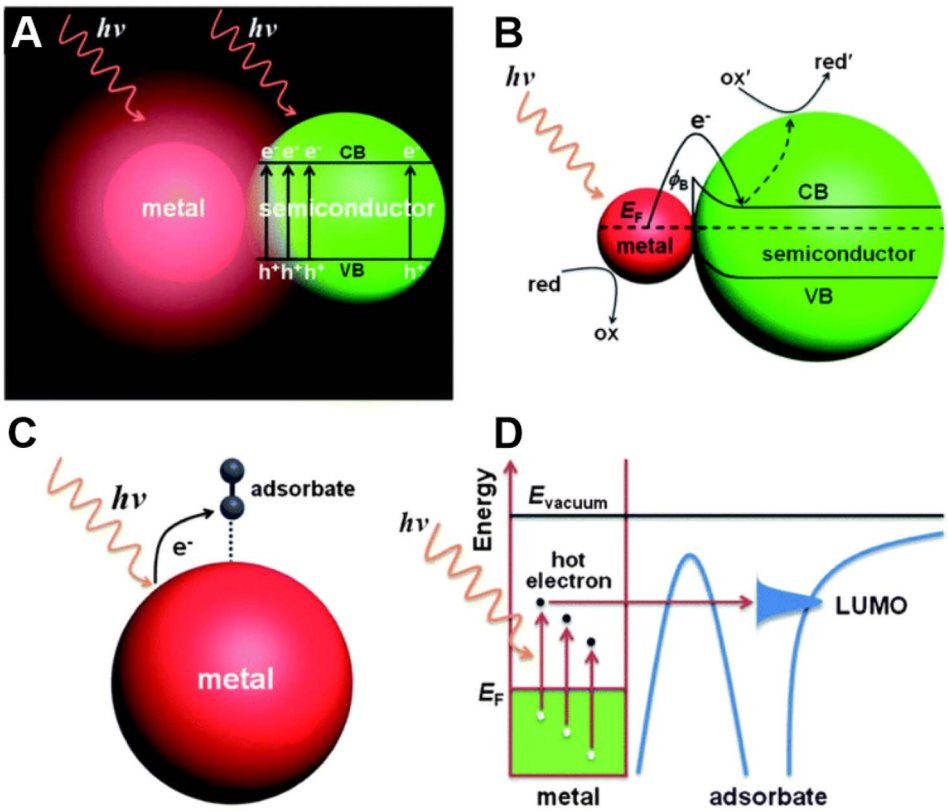

Fig. 3 Schematic representation of the three primary mechanisms through which plasmons facilitate light-driven chemical reactions. (A) Plasmon-enhanced light absorption through intensified near-field effects. (B) Plasmonic sensitization of the semiconductor *via* hot carrier injection. (C and D) Direct photocatalysis on pure metal surfaces driven by plasmon excitation. VB and CB represent the valence band and conduction band of the semiconductor, respectively. E_F denotes the Fermi level at equilibrium. "red" and "ox" indicate the reduced and oxidized forms of a chemical species, respectively. E_{vacuum} refers to the vacuum energy level. Reproduced with permission from ref. 64. Copyright 2013 Royal Society of Chemistry.

absorption spectroscopy, surface-enhanced infrared absorption spectroscopy (SEIRAS), and time-resolved photoluminescence to disentangle and quantify these individual contributions. Additionally, noble metal deposits improve charge separation simply by acting as electron sinks (Schottky junctions) that attract and trap electrons due to the metal's work function.[68] The role of noble metals as electron sinks, well established under ultraviolet illumination through Schottky junction formation, is a classical and non-plasmonic mechanism. In plasmonic photocatalysts, however, this function works in tandem with LSPR-driven processes, collectively enhancing charge separation and suppressing recombination to improve photocatalytic efficiency.

2.2. Photonic crystals and slow photon effects

Photonic crystals are materials that exhibit a periodic variation in the refractive index or dielectric constant at length scales comparable to the wavelength of light.[31–35] This periodic modulation gives rise to a photonic band structure, analogous to the electronic band structure in solids. Within certain frequency ranges known as the photonic bandgap (PBG), light propagation through the crystal is forbidden and is instead completely reflected off the material surface (Fig. 4A). Near the edges of the PBGs, where the light frequency is close to entering or leaving the forbidden range, the dispersion relation flattens such that the frequency of light changes very little even as its wavevector changes. This results in a significant reduction in the group velocity of light, leading to the phenomenon referred to as "slow photons". Within these spectral regions, light is effectively trapped or confined in the structure for longer durations, enhancing light–matter interactions. In 3D PCs, vivid structural colors arise from the photonic stop band, and near the band edges, the optical field forms standing wave patterns due to strong Bragg reflection. A key characteristic of photonic band structures is that at the red-edge of the photonic bandgap, the standing wave exhibits intensity maxima within the high refractive index regions of the material, while at the blue edge, the field intensity peaks are located in the low refractive index regions. This distinction is crucial for photocatalysis. If the active semiconductor constitutes the high refractive index region, aligning its absorption band with the red edge of the photonic bandgap ensures that light is concentrated within the semiconductor itself to enhance photoabsorption. In contrast, blue-edge alignment concentrates light in the low-index or void regions, which could be less effective when the absorbing material is primarily located in the high-index framework.

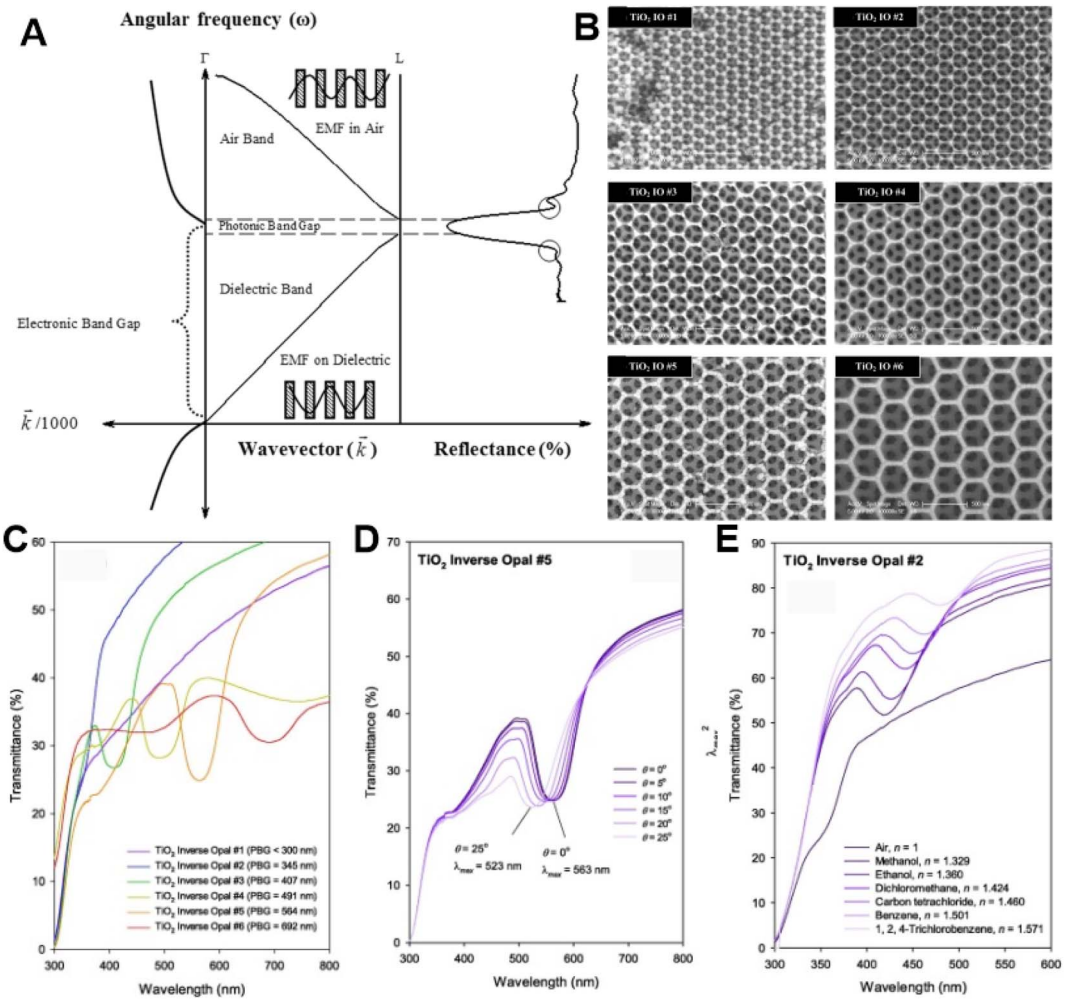

Fig. 4 (A) The left panel shows a plot of angular frequency *versus* wave vector, illustrating the formation of a PBG that can suppress the spontaneous emission of electromagnetic waves by preventing photon propagation within certain energy ranges. The right panel presents the reflectance spectrum of a TiO_2 photonic crystal, indicating the presence of a PBG along the face-centered cubic (111) planes. The circles mark the red and blue edges of the PBG, which can be exploited to enhance light absorption through photonic crystal effects. (B) SEM images of TiO_2 inverse opal thin films with increasing void sizes. UV-visible transmittance spectra of TiO_2 IO thin films showing variations with (C) different void sizes, (D) different angles of light irradiation, and when exposed to (E) different media such as air ($n = 1$), methanol ($n = 1.329$), ethanol ($n = 1.360$), dichloromethane ($n = 1.424$), carbon tetrachloride ($n = 1.460$), benzene ($n = 1.501$), and 1,2,4-tricholorobenzene ($n = 1.571$). Reproduced with permission from ref. 69. Copyright 2016 Elsevier.

Various photonic crystal architectures have been investigated for photocatalytic applications, each offering distinct advantages in light manipulation and catalyst integration. Three-dimensional PCs, such as opal and inverse opal structures, are commonly employed in photocatalysis.[31,35,69] In particular, an inverse opal (IO) PC consists cubic-like porous network of high refractive index material such as TiO_2, where the original templating spheres are etched out to introduce air voids.[70,71] These structures are typically fabricated by infiltrating a colloidal crystal template composed of monodisperse silica or polymer spheres with a material precursor, followed by template removal.[71,72] The resulting material exhibits a highly ordered, three dimensional porous architecture with a tunable photonic stop band, whose position depends on the void size (determined by the diameter of the templating spheres), refractive index contrast, and angle of light irradiation (Fig. 4B–E).[71] For instance, TiO_2 inverse opal has shown its highest dye degradation rate when the PBG overlaps with the dye's absorption band, indicating that slow photons contribute to increased effective light absorption in dye sensitized photocatalysis.[31] Beyond their optical properties, these porous PCs also offer practical advantages such as high surface area and interconnected porosity, which facilitate efficient reactant diffusion and improve photocatalytic performance.

In parallel, one-dimensional photonic crystals (1D PCs) have gained increasing attention as efficient and practical systems for light confinement and enhancement, owing to their simpler fabrication and tunable photonic band structures. These include nanotube arrays, grating waveguide structures, layered

dielectric stacks, and grooved silicon matrices, each offering unique fabrication advantages and optical tuning capabilities.

A widely studied example is TiO_2 nanotube arrays with periodic modulation along their length. By anodizing targeted metal under pulsed or multi-step electrochemical conditions, it is possible to fabricate nanotubes that exhibit periodic variations in diameter, effectively forming a stacked Bragg structure composed of alternating segments with different refractive indices.[73,74] Moreover, in 1D and two-dimensional (2D) TiO_2 nanotube-based PCs, the position of the PBG is closely related to the geometric parameters of the nanotube arrays, specifically, the intertube spacing and wall thickness. These structural features determine the periodic modulation of the refractive index, thereby governing the optical stop band and slow photon behaviour. Similar behavior has been observed in SiO_2/TiO_2 dielectric multilayers with a central defect layer, which supports defect modes within the PBG. These modes shift with changes in the refractive index, enabling sensitive optical responses to environmental conditions or analytes.[75]

In addition, grating waveguide structures, fabricated *via* nanoimprint or interference lithography, represent another class of 1D PCs that support guided-mode resonances (GMRs) with high *Q*-factors.[76] These photonic structures enable sharp resonant confinement of light near the band edge, leading to intensified local electromagnetic fields and prolonged photon–material interaction. The GMR features are highly tunable *via* structural parameters such as the grating period and incident angle, making them versatile for enhancing light absorption and slow photon effects in the visible range.

Tolmachev *et al.*[77] reported on grooved silicon-based 1D PCs, created by wet anisotropic etching of Si (110), which offer high refractive index contrast (Si–air $\sim$3.4 : 1) and support broad PBGs even with few lattice periods. These structures can be infiltrated with liquid crystals to form active composites with tunable optical properties, exhibiting primary and secondary bandgaps across the near- and mid-IR regions. Their large vertical groove depths and compatibility with on-chip photonic integration make them strong candidates for electrically tunable photocatalytic or sensing platforms.

Collectively, these one-dimensional photonic crystal architectures illustrate that slow photon effects can be effectively realized in structurally simpler and more fabrication-friendly configurations. Their compatibility with low-cost, scalable methods such as anodization, lithographic patterning, and wet etching underscores their potential for practical deployment in photocatalytic systems where optical field enhancement and economic viability must be co-optimized.

2.3. Plasmonic–photonic interactions

In a hybrid plasmonic–photonic crystal, the interplay between these two phenomena can yield either enhancement or interference, depending on the spectral and spatial alignment of the modes. The ideal scenario is to "harmonize" the plasmonic and photonic effects so that they constructively reinforce light absorption and charge generation.[45] The goal is to design the photonic crystal to concentrate incident light within the wavelength range where the plasmonic nanoparticles exhibit strong absorption. This can be accomplished by tuning the PBG to align with the plasmon resonance wavelength of the metal nanoparticles. When such spectral matching is achieved, photons at that wavelength are effectively slowed and confined by the PC, increasing their interaction time with the metal nanoparticles and thereby enhancing plasmonic absorption and subsequent photochemical processes. The LSPR of the metal nanoparticles generates strong near fields and energetic charge carriers, which can be injected into an adjacent semiconductor or support scaffold. When the PBG is spectrally aligned with the plasmon resonance, this coupling leads to a synergistic enhancement of photocatalytic activity at the matched wavelengths, exceeding the performance achievable by either the photonic or plasmonic component alone.[78]

Notably, strong synergistic effect was reported for Au-loaded $BiVO_4$ inverse opal photoanodes, in which a polystyrene opal template composed of 260 nm spheres produced a PBG centered near 513 nm.[79] The spectral overlap between the red edge of this PBG and the Au plasmon resonance led to enhanced water splitting performance. It is important to note that if the plasmon resonance and photonic bandgap are not spectrally aligned, the two effects might not help each other and could even hinder performance. Lim *et al.*[46] reported that depositing gold or silver nanoparticles onto a TiO_2 photonic film with a stop band centered around 800 nm, which lies outside the plasmon resonance range of 400 to 550 nm, resulted in reduced photocatalytic activity compared to bare photonic TiO_2. In this case, the PC reflected a portion of the spectrum that did not overlap with the absorption range of the plasmonic nanoparticles, and the addition of metal nanoparticles introduced optical losses without providing any enhancement. This outcome highlights a fundamental design principle in plasmonic–photonic systems, where photonic and plasmonic elements must be carefully integrated to achieve mutual enhancement.

Additionally, 1D photonic crystals offer a powerful platform for synergistic light manipulation when combined with plasmonic nanostructures. The integration of metal nanoparticles (*e.g.*, Au and Ag) onto the surface or within the matrix of 1D PCs enables plasmon–photon coupling, wherein LSPRs interact with slow photon modes or guided resonances supported by the 1D photonic crystal. Liu *et al.*[80] demonstrated that placing Au nanoparticles on dielectric grating waveguides enables tunable plasmon–photon coupling through control of the incident angle, resulting in highly confined fields and sharp resonance features. While integration with TiO_2 nanotube-based 1D PCs has been less extensively reported, emerging evidence suggests that incorporating plasmonic nanoparticles into diameter-modulated nanotube stacks can enhance visible-light absorption and hot electron injection. Such hybridization strategies align slow photon regions with plasmon resonance bands, offering a promising path toward broadband light harvesting and photocatalytic enhancement through spatially engineered optical fields.

Parameters such as the photonic lattice period (which determines the position of the photonic bandgap) and the size,

shape, or material of the nanoparticles (which defines the plasmon resonance wavelength) should be tuned together to ensure effective spectral and spatial coupling. Additionally, the spatial field distribution plays a critical role. For optimal coupling, metal nanoparticles should be positioned within regions of high electromagnetic field intensity associated with the photonic mode. In PCs with periodic refractive index modulation, it is important to consider whether the nanoparticles are embedded within high index regions or located on the surface, relative to the standing wave pattern formed by the photonic structure.

Beyond the slow photon effect in PCs, surface lattice resonances (SLRs) represent a distinct class of collective optical modes that arise in periodic arrays of plasmonic nanoparticles. In 2D plasmonic crystals, regular arrays of metal nanoparticles, the LSPRs of individual particles can couple with in-plane diffracted light, forming hybrid modes known as SLRs. These resonances often exhibit narrower linewidths and stronger field enhancements compared to isolated LSPRs, due to the coherent coupling facilitated by the periodic lattice structure. SLRs have been explored for enhancing light harvesting in applications such as photovoltaics and photocatalysis. For instance, arrays of metal nanodisks with periodic spacing can be designed to support SLRs at target frequencies, thereby extending the lifetime of plasmonic excitations and increasing the generation of hot carriers.[81] This approach leverages the synergistic interaction between plasmonic and photonic modes to improve the efficiency of light-driven processes. While the application of SLRs in photocatalysis is still emerging, the design principles established for plasmonic PCs provide a foundation for future developments. By carefully tuning parameters such as nanoparticle size, shape, and array periodicity, it is possible to manipulate the position of SLRs to align with specific absorption bands of photocatalytic materials and PCs, thereby enhancing their activity through improved light absorption and carrier dynamics.

Overall, these examples illustrate the theoretical foundation of plasmonic PCs, which lies in the integration of localized plasmonic phenomena (*e.g.*, strong near fields and hot carrier generation) with PC effects (*e.g.*, including light trapping through bandgap formation and the generation of slow photons). This synergistic combination enhances light utilization in photocatalytic systems by addressing both photon management and charge activation. The PC component increases the optical path length and prolongs photon residence time within the structure, particularly near photonic band edges where light propagation slows. Simultaneously, plasmonic nanoparticles absorb the confined photons and convert them into energetic charge carriers that can participate in surface reactions. The metallic components also function as co-catalysts, facilitating electron scavenging and supporting multi-electron transfer steps in complex redox processes. With an understanding of these interdependent mechanisms, we now turn to the fabrication of hybrid photonic structures and the design strategies that have emerged to optimize their architecture for improved photocatalytic performance.

3. Fabrication approaches

The fabrication of plasmonic–photonic crystal photocatalysts is a non-trivial challenge because it requires integrating disparate nanoscale components (metals and semiconductors) into a highly ordered structure. Broadly, fabrication approaches can be categorized into bottom–up self-assembly methods or top–down nanofabrication methods, which are often used in combination. In this section, we review current and emerging techniques for creating PCs and incorporating plasmonic elements into them, highlighting both bottom–up (chemical synthesis and templating) and top–down (lithography and etching) strategies.

3.1. Bottom–up fabrication of photonic crystal scaffolds

Bottom–up methods rely on the self-organization of building blocks (*e.g.*, nanoparticles) into an ordered lattice. A notable example is the fabrication of 2D and 3D inverse opal PCs (Fig. 5). The process typically involves three steps: (i) Formation of a colloidal crystal template by self-assembly of monodisperse nanospheres (commonly SiO_2 or polystyrene) into a close-packed lattice.[82–84] This can be achieved by slow sedimentation, vertical deposition, spin coating, or other self-assembly techniques, with careful control to avoid cracks and ensure long-range order.[83–85] (ii) Infiltration of a photocatalyst precursor (*e.g.* a TiO_2 sol or metal–organic precursor) into the interstices of the opal template. Capillary force deposition, drop casting, or vacuum infiltration are often employed to fill the voids completely.[69,72,86] Techniques like sol–gel or atomic layer deposition (ALD) can also be used to conformally coat the template interior.[87] This step is critical, as incomplete infiltration or shrinkage during processing can introduce voids or cracks that compromise the optical quality of the photonic crystal. (iii) The final stage involves removing the template, typically by calcination to decompose polymer spheres or by chemical etching to dissolve silica, resulting in the formation of an inverse opal structure composed of the semiconductor material.[72,86,88,89] Upon successful fabrication, this approach yields a uniform porous PC, typically in the form of a free-standing film or a substrate-supported layer, with periodicity generally in the range of hundreds of nm as determined by the diameter of the templating spheres. This colloidal templating method has been widely employed to construct inverse opals composed of TiO_2, ZnO, and other metal oxides. For example, TiO_2 inverse opals prepared using polystyrene bead templates exhibit well-defined photonic stop bands in the visible region and enhanced photocatalytic dye degradation, attributed to the slow photon effect.[90] The opal templating technique is relatively scalable and cost effective, but it requires high quality monodisperse colloids and careful control over processing conditions to minimize structural defects.[91] In addition, post-assembly thermal treatments have been shown to densify and mechanically reinforce the framework without compromising the long-range order essential for photonic functionality.[84]

Another bottom–up approach to fabricating PCs is the electrochemical growth of 1D PC nanotube arrays. In the case of

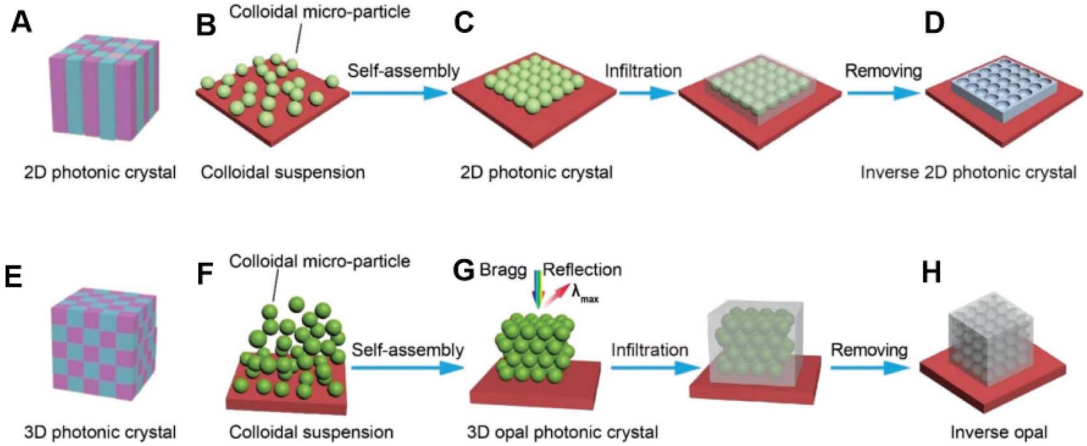

Fig. 5 (A and E) Schematic illustrations of 2D and 3D PC, respectively. (B–D) Self-assembly process of colloidal microparticles to form 2D monolayer PCs and subsequently an inverse-structured crystal after removal of the template. (F–H) Self-assembly process for preparing a 3D opal photonic crystal and inverse opal upon the template removal. Reproduced with permission from ref. 82. Copyright 2006 Elsevier.

anodic TiO_2 nanotubes, periodic modulation of tube diameter or wall thickness can be achieved by altering the anodization voltage in a periodic manner during growth.[74] Zeng *et al.*[92] demonstrated the fabrication of TiO_2 nanotube PCs through precise charge-controlled pulsed anodization, producing vertically aligned nanotubes with periodic modulations along their length and a structural pitch of approximately 100 nm. This method yields a pronounced 1D photonic bandgap in the visible range without requiring colloidal templating. The resulting structures combine the benefits of highly ordered nanotube arrays such as large surface area and efficient charge transport pathways with slow photon effects that enhance light absorption. When decorated with gold nanoparticles, these PCs formed plasmonic–photonic hybrid architectures that exhibited improved CO_2 photoreduction activity. The enhancement was attributed to the spectral overlap between the photonic bandgap and the LSPR of the gold nanoparticles, which extended photon residence time and increased hot carrier utilization. While the anodization process offers a simple and scalable route to structured photonic materials, it requires careful control over electrochemical parameters. Moreover, the periodic modulation is sensitive to post-treatment conditions such as thermal annealing, which must be optimized to preserve the photonic features.

3.2. Top–down nanofabrication

Top–down fabrication techniques involve carving or patterning a material using lithography or etching to create a multidimensional periodic structure. These methods offer high precision and the ability to design more complex or arbitrary photonic patterns (*e.g.*, beyond the natural close-packed geometry of opals), although often at higher cost or smaller scale. One common top–down approach for 2D PCs is nanolithography on semiconductor films. For instance, nanoimprint lithography or interference lithography can define a periodic array of holes or pillars in a resist, which is then transferred into a photocatalyst film (*e.g.*, TiO_2) by etching.[50] Torras *et al.*[50] developed a soft nanoimprint lithography technique to pattern a mesoporous TiO_2 film into a 2D PC slab featuring a square lattice of pores (Fig. 6A and B). The mesoporous nature of TiO_2 provided a high surface area beneficial for photocatalytic reactions, while the imprinted periodic structure enabled in-plane diffraction and efficient light coupling into the film. This method offers good scalability, as single-step imprinting can pattern areas on the order of square cm, and it is compatible with conductive substrates, making it suitable for photoelectrode fabrication.

Electron-beam lithography (EBL) was used to fabricate 2D photonic crystal structures with feature sizes ranging from submicron to millimeter scales. Using a cumulative dose technique, the authors patterned periodic arrays by superimposing orthogonal line patterns with a line dose of 125–150 nC m^{-1} onto a 400 nm PMMA resist layer.[93] Similarly, PCs were patterned into the top silicon layer of silicon-on-insulator substrates, forming triangular lattices with a 500 nm period and hole diameters tunable from 250 to 465 nm by varying the exposure dose between 350 and 650 μC cm^{-2} (Fig. 6C and D). In parallel, nanoimprint molds were fabricated *via* EBL-defined nickel masks and reactive ion etching to a depth of ~200 nm, enabling high-fidelity thermal imprinting of photonic structures at 140 °C and a pressure of 80 bar (Fig. 6E and F).[94] The resulting PCs consisted of dot arrays and hole arrays with pitches and geometries suitable for manipulating light in the visible and near-infrared ranges. Overall, structures such as titanium island arrays on glass and resist hole arrays on silicon were successfully produced, demonstrating the versatility of EBL in tailoring PC architectures for different substrates and optical applications. Notably, Matsushita *et al.*[95] designed a rutile-phase TiO_2 PC with triangular lattices of square rods connected by walls, achieving large complete photonic bandgaps suitable for light management in solar energy devices. Although EBL offers exceptional control over nanoscale patterning, it remains time-consuming and costly for large-area fabrication.

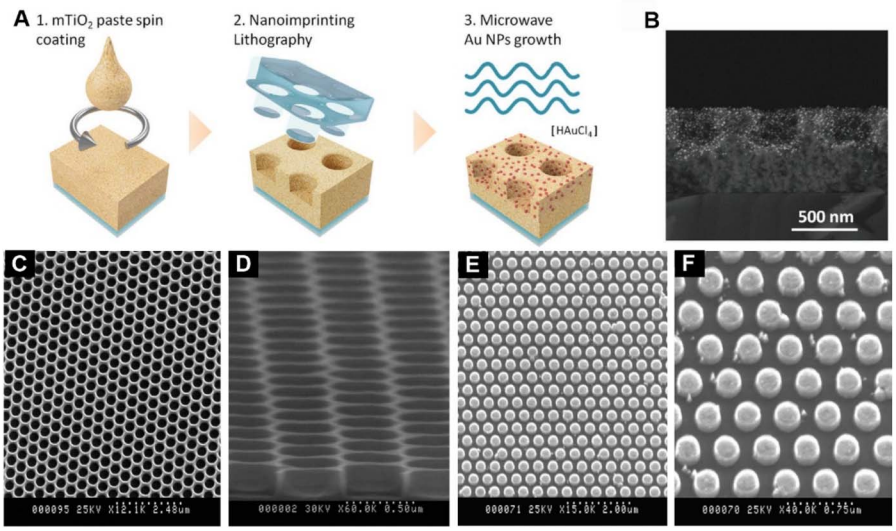

Fig. 6 (A) Fabrication scheme and (B) SEM cross-sectional image of the nanostructured photocatalytic TiO_2 photonic crystal substrates formed by using a lithography-based approach. Reproduced with permission from ref. 50. Copyright 2021 Wiley. SEM images of (C and D) silicon on insulator photonic crystals with a 500 nm lattice constant and (E and F) silicon nanoimprint molds fabricated by electron beam lithography. Reproduced with permission from ref. 94. Copyright 2004 Elsevier.

Laser interference lithography (LIL) is a parallel technique in which interfering laser beams create a periodic intensity pattern to expose a resist, enabling wafer-scale patterning of gratings or 2D lattices in a single exposure. LIL has been used to fabricate 3D woodpile PCs through multiple exposures or multi-photon direct laser writing; however applying this approach to metal oxides often requires some replication steps (writing a polymer scaffold then backfilling with TiO_2, *etc.*).[96] Similarly, multi-photon direct laser writing (DLW), also known as two-photon polymerization, allows for the fabrication of complex 3D photonic structures with sub-micrometer resolution. In this approach, a focused femtosecond laser induces localized polymerization within a photosensitive material, creating intricate 3D scaffolds. These polymer templates can then be infiltrated with TiO_2 using techniques like atomic layer deposition, followed by removal of the polymer to yield high-refractive-index TiO_2 PCs.[97] While LIL offers rapid and scalable patterning suitable for large-area applications, it is generally limited to planar structures. In contrast, DLW provides unparalleled design flexibility for 3D architectures but it is more time-consuming and less suited for large-scale production.[98]

Porous anodic alumina (PAA) templates also merit mention as a quasi-top–down method.[99,100] Self-ordered PAA forms a hexagonal array of nanopores in aluminum oxide, which can function as a 2D PC or as a template for further material replication. Semiconductor materials such as titania can be deposited into the pores or onto the surface to construct photonic architectures.[46] For instance, a TiO_2-coated nanoporous anodic alumina framework has been utilized as an inverse opal photonic crystal scaffold for the integration of plasmonic nanoparticles. Although in this case the photonic and plasmonic resonances were spectrally mismatched, resulting in diminished photocatalytic activity, the method itself remains a robust and scalable route for fabricating mechanically stable photonic crystal films.

3.3. Incorporating plasmonic nanoparticles

Once the photonic crystal scaffold of a semiconductor such as titanium dioxide is fabricated using one of the aforementioned methods, the next step is the incorporation of plasmonic metal nanoparticles into the framework. This integration must be performed carefully to preserve both the photonic order (which could be disrupted by large inclusions or film deposition) and the plasmonic integrity (metal nanoparticles should remain well-dispersed and not overly damped by oxidation or sintering). Several approaches have been employed, including (1) infiltration with colloidal nanoparticles, (2) *in situ* photodeposition or chemical reduction, (3) hydrothermal growth of nanoparticles, and (4) direct nanofabrication of plasmonic structures on photonic substrates.

One common approach is infiltration with colloidal nanoparticles. This involves immersing the pre-formed photonic crystal scaffold in a colloidal solution containing pre-synthesized metal nanoparticles, such as gold or silver sols.[69,101,102] Capillary forces facilitate the penetration and uniform distribution of the nanoparticles within the porous photonic crystal network, ensuring effective interfacial contact and strong optical coupling between the plasmonic and photonic components.[45] However, achieving uniform infiltration deep into a 3D photonic crystal can be challenging, and it is essential to immobilize the nanoparticles to prevent leaching or aggregation. Often, a subsequent step such as thermal treatment is necessary to immobilize the nanoparticles within the photonic crystal framework. However, this process can induce undesirable oxidation, particularly in the case of silver nanoparticles.[103] Erola *et al.*[104] systematically compared co-assembly and post-infiltration strategies for incorporating gold and silver nanoparticles into a silica opal template. In the co-

assembly method, positively charged gold nanoparticles were mixed with silica spheres prior to opal formation, resulting in a homogeneous distribution of gold throughout the structure. However, this approach proved unsuitable for silver, as the subsequent calcination step led to the oxidation of metallic silver (Ag^0) to silver oxide (Ag_2O), thereby suppressing the localized surface plasmon resonance. In contrast, the post-infiltration approach where metal nanoparticles were introduced after forming the photonic titanium dioxide structure was more effective in preserving silver in its metallic state. The study concluded that the thermal stability of the metal is a critical factor; gold, with its higher melting point and lower susceptibility to oxidation, can sometimes be incorporated *via* co-assembly, whereas silver requires milder processing conditions and post-synthetic incorporation to retain its plasmonic functionality.

In situ photodeposition is an effective technique for integrating metal nanoparticles into PCs, involving the *in situ* formation of nanoparticles from metal salt precursors within the porous structure using light. For instance, filling the pores of a titanium dioxide inverse opal with an aqueous solution of chloroauric acid ($HAuCl_4$) followed by ultraviolet (UV) illumination can induce photoreduction, leading to the nucleation of gold nanoparticles anchored on the TiO_2 surfaces. Similarly, infiltrating silver nitrate ($AgNO_3$) into the TiO_2 framework and subsequently utilizing the photocatalytic properties of TiO_2 under illumination can yield silver nanoparticles. This photodeposition process leverages the photogeneration of electrons in TiO_2 under UV light to reduce metal ions to metallic nanoparticles *in situ*.[105] Such methods have been successfully employed to decorate TiO_2 inverse opals with platinum, gold, and silver nanoparticles without disrupting the periodic opal structure.[48,105–107] The advantage of this approach lies in achieving a uniform coating of nanoparticles directly on the internal surfaces of the photonic crystal, ensuring good interfacial contact. Moreover, the metal loading can be tuned by adjusting the concentration of the precursor solution and the duration of illumination. However, it is crucial to ensure that the photonic crystal structure remains intact under reaction conditions, as excessive UV exposure or heat generated during the process could potentially damage or fracture the delicate framework.

Hydrothermal growth offers a solution-based approach for depositing plasmonic nanoparticles within photonic crystal frameworks, enabling controlled nucleation and strong interfacial contact under controlled temperature and pressure conditions. Lu *et al.*[78] reported a hydrothermal strategy for anchoring gold nanoparticles onto a titanium dioxide photonic crystal, wherein partial interfacial sintering enhanced nanoparticle adhesion and structural stability. In this method, the photonic crystal scaffold such as a TiO_2 inverse opal is dispersed in an aqueous solution containing a gold precursor and subjected to hydrothermal conditions (elevated temperature and pressure), promoting the *in situ* nucleation and growth of gold nanoparticles directly on the TiO_2 framework. Mild sintering at the interface fosters strong binding between the nanoparticles and the TiO_2 matrix, which helps prevent nanoparticle detachment during operation. However, excessive sintering must be avoided to preserve both the photonic band structure and the localized surface plasmon resonance of the metal nanoparticles.

Apart from this, direct nanofabrication provides a top–down strategy to integrate plasmonic structures onto photonic crystal substrates with high spatial precision, allowing the creation of periodic metal patterns that align with the underlying photonic architecture. This method involves the direct patterning of plasmonic nanostructures onto pre-formed photonic crystal substrates using top–down nanofabrication techniques. For instance, after creating a 2D photonic crystal pattern in titanium dioxide *via* lithography, electron beam lithography can define an array of metal nanodisks, or a metal film can be deposited and subsequently etched to form a plasmonic lattice that aligns with the dielectric pattern. Torras *et al.*[50] demonstrated a scalable approach using soft nanoimprint lithography to fabricate Au/TiO_2 2D PCs. In their first process, gold nanoparticles were *in situ* infiltrated into the superficial ~50 nm of a mesoporous TiO_2 scaffold patterned with a photonic structure, creating a plasmonic pattern that followed the photonic lattice. In a second variant, they achieved a homogeneous distribution of Au colloids throughout the volume of the photonic crystal by mixing colloidal Au with the sol before imprinting. This hybrid bottom–up/top–down method allowed for patterning over large areas, and the *in situ* incorporation of Au ensured that every photonic crystal "cell" contained plasmonic content. The study highlighted the importance of controlling lattice parameters, geometry, and metal loading to optimize optical properties.

Additionally, magnetron sputtering is also a versatile physical vapor deposition technique commonly used to introduce plasmonic nanoparticles onto photonic crystal surfaces with precise control over thickness and composition. This method enables uniform deposition of metals such as Au or Ag onto the photonic scaffold, facilitating strong plasmon–photon coupling for enhanced photocatalytic performance. One of the reported studies demonstrated that Au nanoparticles were deposited onto periodically modulated TiO_2 nanotube PCs (PMTiNTs) using direct current magnetron sputtering at 75 W for 1 minute, without substrate heating. This sputtering method enabled uniform Au nanoparticle loading (~85 μg per 6.25 cm^2 sample), with particle sizes averaging ~4.9 nm, facilitating strong plasmon–photon interactions critical for enhanced photocatalytic activity (Fig. 7).[92]

Maintaining the long-range periodicity of PCs after incorporating metal nanoparticles is crucial for preserving their optical properties. Harsh treatments, such as high-temperature calcination required for crystallizing TiO_2, can induce cracks or grain growth and disrupt the periodic order. Similarly, excessive metal loading may introduce disorder, compromising the structural integrity of the PC. Experimental observations underscore the importance of preserving the photonic lattice's structure. For instance, a biomorphic TiO_2 PC decorated with Au nanoparticles exhibited drastically reduced dye photocatalytic degradation efficiency when ground into a powder, compared to its intact monolithic form.[102] Although the powdered form still outperformed a random Au/TiO_2 reference, the loss of periodicity led to diminished performance. These

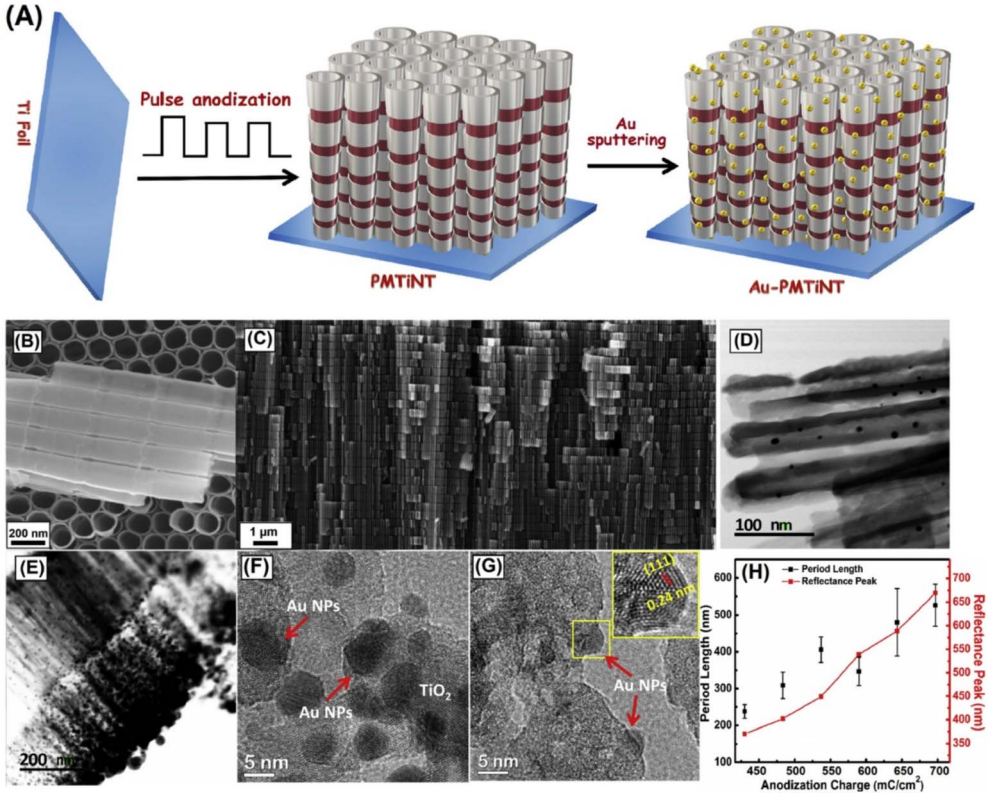

Fig. 7 (A) Schematic illustration of the fabrication process for PMTiNT arrays. (B and C) Top-view and cross-sectional FESEM images of the as-prepared PMTiNT structure, respectively. (D and E) TEM images of Au-loaded PMTiNTs, showing the distribution of gold nanoparticles. (F and G) HRTEM images highlighting the gold nanoparticles and their lattice fringes. (H) Dependence of the photonic crystal pitch (defined as the length of the repeating periodic segment) and the corresponding optical reflectance peak on the anodization charge, demonstrating the tunability of photonic bandgaps through charge-controlled anodization. Reproduced with permission from ref. 92. Copyright 2020 Elsevier.

findings highlight that preserving the periodic architecture, even when scaling down to powder form, is essential for harnessing the photonic benefits. Consequently, advanced fabrication techniques focus on gentle integration methods and post-processing steps that avoid lattice damage, ensuring the structural and functional integrity of PCs.

3.4. Emerging techniques

As the field of photonic–plasmonic hybrid materials advances, several innovative fabrication methods are being explored to overcome current limitations and enhance the performance of photocatalytic systems. Two-photon polymerization (2 PP) has emerged as a powerful additive manufacturing technique, enabling the fabrication of complex 3D photonic crystal geometries with sub-micron resolution. This method allows for the creation of intricate structures that can broaden photonic bandgaps and tailor optical properties. For instance, researchers have demonstrated the use of 2PP to fabricate woodpile PCs, which after a controlled heat-shrinking process, exhibit vibrant structural colors due to their PBG properties.[108] In parallel, block copolymer self-assembly and DNA-origami techniques are gaining attention for constructing ordered photonic and plasmonic arrays.[109,110] While not yet widely applied in photocatalysis, DNA-assembled plasmonic arrays offer exceptional control over nanoparticle positioning, and block copolymers provide scalable routes to nanostructures with tunable periodicity. Efforts are also growing in scalable soft-lithography methods, which allow large-area patterning of photonic structures on flexible substrates—paving the way for roll-to-roll production of photocatalytic sheets and coatings.[50] These approaches are particularly attractive for practical applications due to their compatibility with low-cost, high-throughput manufacturing. Another frontier involves the integration of reconfigurable elements into photonic architectures. For instance, recent studies demonstrated optically tunable Tamm plasmon–polariton crystals, where a tunable phase-change material enabled dynamic modulation of the photonic–plasmonic coupling.[110] Although originally developed for display technologies, similar concepts could be adapted to create photocatalytic platforms with on-demand tunable bandgaps, responsive to solar spectral changes or varying reaction conditions. Collectively, these innovations represent a shift toward more versatile, adaptive, and scalable photonic–plasmonic systems designed for next-generation photocatalytic applications.

Clearly, the effective fabrication of plasmonic–photonic crystal photocatalysts requires adapting techniques from colloid chemistry, nanofabrication, and materials science. Bottom–up methods excel at producing high-quality 3D PCs (like inverse opals and nanotube PCs) economically, whereas

top–down methods provide design flexibility (especially for 2D patterns and integrated devices). Often a hybrid approach, such as self-assembling a structure followed by metal incorporation through infiltration or light-directed metal deposition is used. The successful fabrication of these hybrids is evident in the growing number of reports demonstrating intact photonic bandgaps alongside plasmonic absorption in the final materials. With robust fabrication strategies in hand, researchers have been able to tune and improve the designs, as discussed next.

4. Design advancements

Early studies on plasmonic–photonic crystal photocatalysts established the basic feasibility and benefits of combining slow photons with LSPR. Building on this foundation, recent research has focused on refining the structural and material design to maximize light–matter interactions, extend the active photoabsorption range, and facilitate charge separation for targeted reactions. In this section, we highlight several key advancements in design focusing on spectral tuning strategies, novel material combinations, architecture optimizations for charge dynamics, and techniques to broaden the overall photocatalytic response.

4.1. Spectral matching and tuning

A primary design goal is to ensure that the PBG of the crystal and the plasmonic resonance of the metal are spectrally aligned, as emphasized in Section 2. Initial demonstrations often involved trial-and-error in choosing sphere sizes (for opals) or nanoparticles sizes. Today, improved quantitative understanding enables more deliberate tuning. For example, slow photons at the red edge have been identified as more effective for interaction with absorbers in the high-index backbone.[31,69,78,111,112] Thus, researchers now often target the red-edge of the photonic stop band to coincide with the metal LSPR. This can be achieved by slightly adjusting the lattice constant of the PC (*e.g.*, using a slightly larger or smaller sphere template or etching the opal to shift the PBG) such that the red-edge aligns with the plasmonic metal's LSPR. Notably, an even greater enhancement was achieved when the plasmon resonance of gold nanoparticles was aligned with the red edge of the photonic bandgap. Zhang *et al.*[111] demonstrated that tuning the Au LSPR to overlap with the red edge (approximately 518 nm) of a TiO_2 nanorod array PC resulted in a higher photoelectrochemical water splitting current compared to blue edge alignment. In both cases, red edge coupling proved more effective, consistent with theoretical predictions that the red edge optical field is concentrated in the high refractive index TiO_2, where the plasmonic nanoparticles are embedded. Apart from that, Lu *et al.*[78] successfully fabricated a TiO_2 PC using a templating approach with 240 nm polystyrene spheres, forming a periodic porous structure upon template removal. Subsequently, ~15 nm Au nanoparticles were uniformly infiltrated into the porous TiO_2 matrix, enabling effective plasmon–photonic coupling throughout the scaffold (Fig. 8A and B). A precisely tuned Au–TiO_2 inverse opal was developed where the Au LSPR (~520 nm) overlapped with the blue-edge of the TiO_2 photonic bandgap, achieving a 2.3-fold higher pollutant degradation rate under visible light compared to a non-photonic reference catalyst (Fig. 8C–E). This study shows that while blue-edge slow photons are generally less effective than red-edge photons in enhancing light–matter interactions, they can still provide meaningful photocatalytic enhancement by selectively amplifying optical transitions near the PBG (Fig. 8F). Simultaneously, the size and morphology of metal nanoparticles can be precisely controlled to modulate the wavelength position of their LSPR.

Additionally, bimetallic plasmonic nanoparticles introduce an additional degree of tunability. For example, gold–silver alloys or core–shell architectures enable continuous adjustment of the plasmonic resonance wavelength between that of pure silver and pure gold. Such bimetallic systems can also exhibit multiple plasmonic modes. Gold–silver alloy nanoparticles, for instance, display tunable resonances in the range of approximately 450 to 600 nm, depending on their compositional ratio.[113] Incorporating these bimetallic nanoparticles into PC architectures allows improved spectral overlap with specific photonic bandgaps compared to monometallic counterparts. Furthermore, shape-controlled nanoparticles such as gold nanorods or bipyramids possess multiple plasmonic modes, typically longitudinal and transverse, and offer broader spectral tunability.[59] These anisotropic particles can be strategically selected to couple with higher-order photonic bands or multi-band photonic structures, thereby enhancing light–matter interactions across a wider spectral range.

Researchers have been exploring advanced PC architectures to broaden the spectral range of light–matter interactions, particularly for applications in photocatalysis. One promising strategy involves the design of hierarchical or multilayer PCs that exhibit multiple photonic stop bands. For example, bilayer inverse opal structures with differing periodicities can produce slow photon regions across distinct wavelength ranges, thereby enhancing light absorption over a wider spectral window. This concept was demonstrated by Madanu *et al.*[114] through the synthesis of TiO_2@$BiVO_4$ IO bilayer architectures to achieve broadband optical enhancement. Incorporating plasmonic nanoparticles, such as silver and gold, into these structures can further optimize the overlap between plasmonic resonances and photonic bandgaps, thereby improving photocatalytic efficiency.

Another innovative approach is the implementation of graded PCs, where the lattice constant varies spatially within the structure.[115] This gradation leads to a continuous shift in the PBG across the material, effectively broadening the slow photon effect over a wider wavelength range. While this method may introduce some loss of coherence compared to a uniform PC, it offers a valuable trade-off by extending the operational bandwidth, which is particularly beneficial for harvesting a more significant portion of the solar spectrum. These advanced photonic crystal designs underscore the importance of structural engineering in tailoring optical properties for enhanced light–matter interactions. By leveraging multilayer configurations and graded structures, researchers aim to

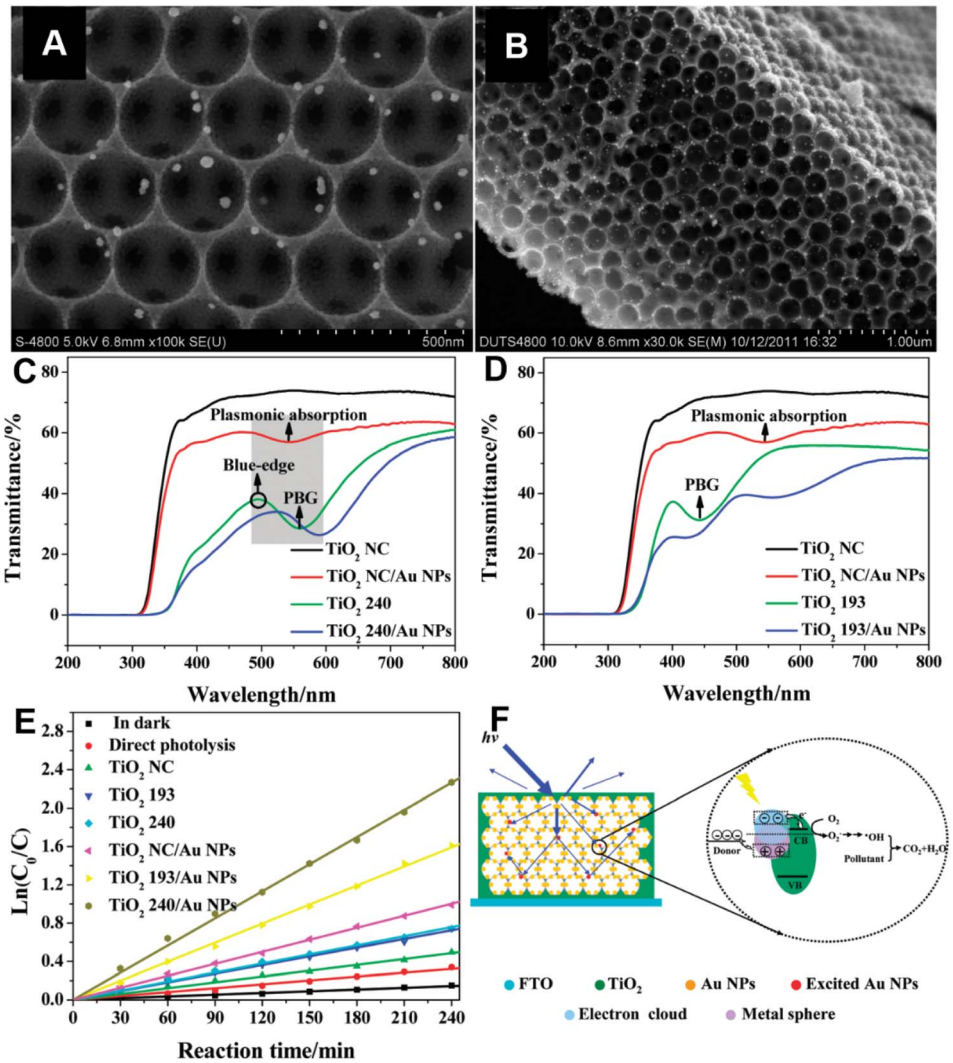

Fig. 8 SEM images of TiO_2 240/Au NPs from (A) top view and (B) cross section view. Transmittance spectra of (C) TiO_2 240/Au NPs and (D) TiO_2 193/Au NPs. The shaded area highlights the spectral overlap between the photonic bandgap of TiO_2 240 and the plasmonic absorption of the Au nanoparticles, while the circle marks the blue edge of the photonic bandgap. (E) Performance kinetics plot of 2,4-DCP degradation using various platforms under visible light (λ > 420 nm) irradiation. (F) Schematic illustration of the pollutant's degradation mechanism using TiO_2 PC/Au NPs. Reproduced with permission from ref. 78. Copyright 2012 American Chemical Society.

develop photocatalytic systems with improved efficiency and broader applicability in solar energy conversion.

Building on these strategies, a notable recent advancement involves employing a non-absorbing photonic crystal backbone, which helps to eliminate optical competition with the semiconductor's intrinsic absorption. This design choice allows the photonic structure to enhance light management without interfering with the active material's photon harvesting capabilities. An illustrative example of this approach was reported by Raja Mogan *et al.*[45] Instead of the commonly used UV-absorbing TiO_2 semiconductor, an optically inert SiO_2 opal photonic crystal framework was employed to support plasmonic enhancement. This non-absorbing scaffold was then functionalized with plasmonic silver nanoparticles, enabling enhanced light manipulation without introducing additional absorption losses from the backbone material. The idea was that SiO_2 does not absorb visible light at all, so it purely serves to trap and localize light *via* photonic effects without interfering with the absorption of photons by the plasmonic metal. Consequently, this optical effect generates a stronger plasmon resonance on the Ag nanoparticles, which then directly drive efficient hydrogen evolution. By aligning the SiO_2 opal's PBG with the Ag LSPR, we achieved a remarkable >10^6-fold enhancement in the H_2 generation rate compared to bare Ag nanoparticles, resulting in significantly enhanced performance compared to reported systems where TiO_2 or other light-absorbing semiconductors were used as the main photonic crystal framework. This work suggests that when the photonic structure itself does not compete for absorption, the plasmonic effect can be maximized. In contrast, conventional photocatalytic PC architectures using semiconductor supports often absorb part of the incident light without contributing effectively to plasmonic activation. This is particularly limiting when the semiconductor possesses a narrower bandgap (*e.g.*, ~2.5 eV), as it can absorb

visible photons and generate electron–hole pairs that may be less efficiently utilized than plasmon-derived hot carriers in certain reaction pathways. This approach eliminates the need for a light-absorbing semiconductor, relying instead on the PC purely as light-trapping scaffolds while plasmonic nanostructures serve as the active sites for photocatalytic transformation.

4.2. Materials and composition innovations

While Au and Ag on TiO_2 have been the prototypical system, researchers are expanding the palette of materials for both the plasmonic and photonic components. Firstly, researchers are exploring different plasmonic metals. Gold and silver nanoparticles are renowned for their strong LSPRs in the visible spectrum, making them highly effective in enhancing photocatalytic processes. However, the high cost of Au and the susceptibility of Ag to oxidation limit their practical applications. As alternatives, copper and aluminum nanoparticles have been explored due to their plasmonic resonances in the visible and ultraviolet regions, respectively. Despite their broader resonance peaks resulting from higher intrinsic losses, these metals offer cost-effective and abundant options for plasmon-enhanced photocatalysis. Recent studies have demonstrated the incorporation of Cu nanoparticles into TiO_2-based PC structures to facilitate CO_2 reduction. For instance, Cu-decorated TiO_2 nanorod films have shown enhanced photocatalytic activity under UV light, attributed to the LSPR effect of Cu nanoparticles, which improves light absorption and charge separation efficiency.[116] Zhang *et al.*[117] reported the fabrication of copper nanoparticle-decorated TiO_2 nanotube arrays *via* pulsed electrochemical deposition, resulting in a plasmon-enhanced photocatalyst responsive to visible light. The optimized Cu/TNAs-20 sample achieved a hydrogen evolution rate of 3.0 mmol h^{-1} cm^{-2}, which was 10.7 times higher than that of bare TiO_2 nanotubes, highlighting the effectiveness of copper plasmonic enhancement and the system's excellent photoelectrochemical stability. Additionally, the construction of photonic crystal/Cu^{2+}-doped TiO_2–SiO_2 composite films has been reported to exhibit superior photocatalytic performance, leveraging the synergistic effects of PBG-induced light trapping and Cu-induced charge carrier dynamics.[118]

Platinum (Pt), traditionally known for its broad interband absorption rendering it gray-black in bulk form, exhibits plasmonic behavior at the nanoscale, particularly in the ultraviolet-visible range, albeit with broader and less intense resonances compared to gold or silver. In a study by Qin *et al.*,[119] a hierarchical nanostructure comprising large Pt nanoparticles supported on TiO_2 was prepared, resulting in a broad visible light absorption tail attributed to Pt's plasmonic properties. This Pt/TiO_2 architecture demonstrated efficient overall water splitting under visible light irradiation, highlighting Pt's dual functionality as both a plasmonic light absorber and an effective co-catalyst for hydrogen and oxygen evolution reactions. Jiao *et al.*[120] developed a series of Pt nanoparticle-decorated TiO_2 PCs (Pt_x/PC-TiO_2) using a gas bubbling-assisted membrane reduction method, achieving a uniform Pt nanoparticle distribution (~2.6 nm) within the inverse opal framework (Fig. 9A–C). The optimized Pt_4/PC-TiO_2 catalyst exhibited excellent CH_4 production of 2.416 mmol in 450 minutes, 2.4 times higher than that of pure TiO_2 PCs (PC-TiO_2) and 3.2 times greater than that of commercial P25, demonstrating the synergistic effects of the slow-photon structure and plasmon-enhanced charge separation (Fig. 9D and E). The demonstrated effectiveness of the plasmonic Pt system indicates that other bifunctional metals, such as palladium[121] or selected bimetallic alloys, hold potential to act simultaneously as plasmonic light absorbers and active catalytic sites. This integrated functionality could simplify photocatalyst architectures by removing the requirement for separate co-catalysts, thereby improving overall efficiency and facilitating more straightforward material fabrication.

Plasmonic semiconductors, particularly heavily doped metal oxides and copper chalcogenide nanocrystals, represent a promising frontier in photocatalysis by combining light absorption, plasmonic effects, and catalytic activity within a single material. Materials such as tungsten-doped TiO_2 and oxygen-deficient WO_3 can support LSPRs in the infrared region due to high free carrier concentrations. These LSPRs can be tuned by adjusting doping levels, enabling the extension of photocatalytic activity into the infrared spectrum. For instance, aliovalent doping in metal-oxide nanocrystals has been shown to produce tunable infrared LSPRs, enhancing light absorption capabilities.[122,123] Additionally, copper chalcogenide nanocrystals (*e.g.*, $Cu_{2-x}S$ and $Cu_{2-x}Se$) exhibit plasmonic behaviour in the near-infrared to mid-infrared range due to copper vacancies that introduce free hole carriers. These materials can be synthesized with controlled stoichiometry to fine-tune their plasmonic properties. Hybrid structures combining noble metals with copper chalcogenides (*e.g.*, Au@$Cu_{2-x}Se$) have demonstrated dual plasmonic resonances, enhancing light–matter interactions and photocatalytic efficiency.[124] Incorporating these plasmonic semiconductors into photonic architectures, such as inverse opal structures, can further enhance light absorption and catalytic activity. The PC environment can slow down light propagation, increasing the interaction time between light and the plasmonic material, thereby boosting photocatalytic reactions. The convergence of plasmonic and catalytic functionalities in these semiconductors blurs the traditional distinction between light-harvesting and catalytic components, paving the way for more efficient and simplified photocatalytic systems.[125]

Apart from commonly used semiconductors such as TiO_2, narrower-bandgap semiconductors like $BiVO_4$ (bandgap ~2.4 eV) have been structured into inverse opal PC to enhance visible light absorption for water oxidation. Incorporating Au nanoparticles into these $BiVO_4$ inverse opals leverages the slow photon effect where reduced group velocity near the photonic stopband edge increases light–matter interaction and the LSPR of Au nanoparticles to boost photocatalytic performance. Specifically, Au–$BiVO_4$ inverse opal photoanodes achieved an oxygen evolution rate of 9.56 μmol cm^{-2} h^{-1}, approximately three times higher than that of pure $BiVO_4$ inverse opals, due to enhanced light absorption and improved charge carrier separation facilitated by the synergistic effects of the photonic

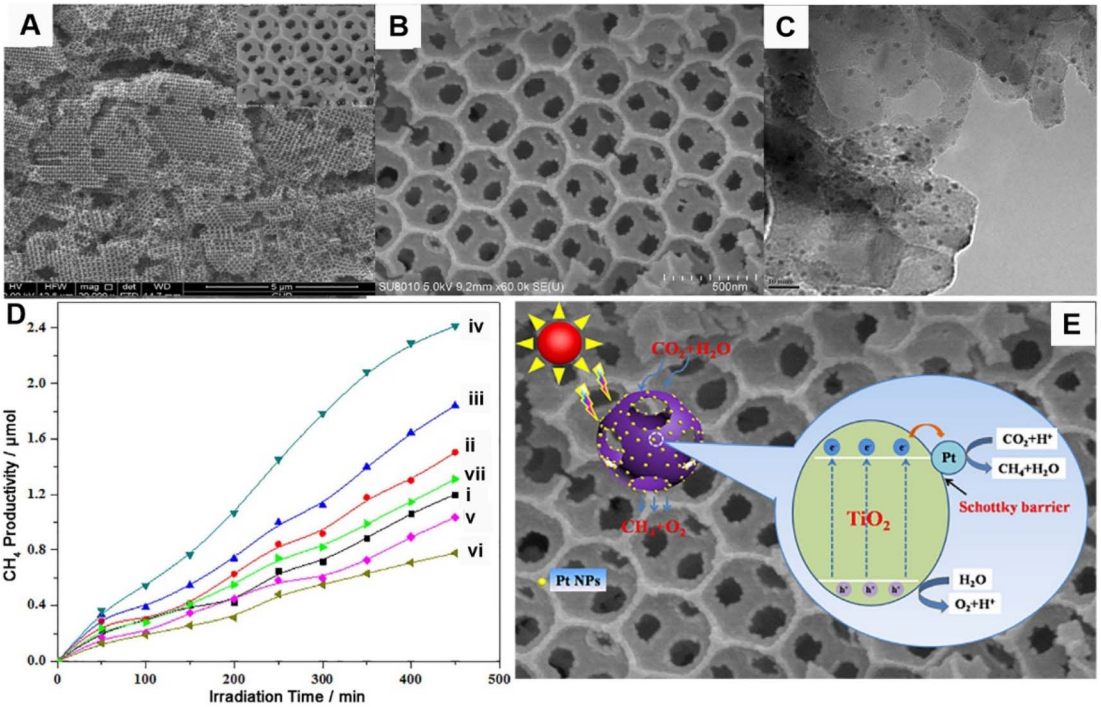

Fig. 9 SEM images of (A) PC-TiO_2 and (B) Pt_4/PC-TiO_2. (C) TEM image of Pt_4/PC-TiO_2. (D) CH_4 production amounts of P25 and Pt_x/PC-TiO_2 catalysts: (i) $Pt_{0.5}$/PC-TiO_2, (ii) Pt_1/PC-TiO_2, (iii) Pt_2/PC-TiO_2, (iv) Pt_4/PC-TiO_2, (v) PC-TiO_2, (vi) P25, and (vii) particle-type Pt_4/TiO_2. (E) Proposed mechanism of the enhanced photocatalytic activity of Pt_x/PC-TiO_2. Reproduced with permission from ref. 120. Copyright 2017 Wiley.

structure and plasmonic Au nanoparticles.[52] Another promising semiconductor is graphitic carbon nitride (g-C_3N_4), which has attracted attention for visible-light-driven photocatalysis due to its suitable bandgap and metal-free composition. While Au-decorated g-C_3N_4systems have shown enhanced CO_2 conversion through improved charge separation and CO_2 activation, studies specifically combining Au nanoparticles with inverse opal-structured g-C_3N_4 remain limited.[126,127] This integration could synergistically couple photonic light trapping and plasmonic enhancement with the chemical effects rendered by g-C_3N_4, offering a yet underexplored avenue for high-performance CO_2 photocatalysis.

Recent studies have explored ZnO and Fe_2O_3 photonic crystal architectures integrated with plasmonic nanoparticles for targeted photocatalytic applications. Meng *et al.*[51] reported that Au-decorated ZnO PCs (Au/ZnO-PC) achieved an enhanced Rhodamine B degradation rate under visible light, 24.8 times higher than that of commercial ZnO and 5.6 times higher than that of N-doped TiO_2. The enhanced performance was attributed to the combined effects of photonic bandgap-induced light confinement and plasmon-mediated charge separation. Additionally, the incorporation of plasmonic nanoparticles, such as silver or gold, onto Fe_2O_3 nanostructures has been shown to further augment photo-Fenton activity. This enhancement is due to the LSPR effect, which increases light absorption and promotes the generation of reactive oxygen species. For example, the decoration of Fe_2O_3 nanowires with non-contacted Au nanoparticles within confined spaces has led to promoted photo-Fenton reactivity through efficient electron transfer mechanisms.[128] These findings underscore the potential of combining PC structures with plasmonic nanoparticles to develop highly efficient photocatalysts for environmental remediation applications.

An effective strategy to improve charge separation in plasmonic–photocatalytic systems involves the use of core–shell nanostructures, where a plasmonic core is encapsulated within a semiconductor shell to form a direct heterojunction. A representative example is Au@TiO_2 core–shell nanoparticles, in which the gold core generates LSPR under visible light, while the surrounding TiO_2 shell efficiently captures hot electrons. In a study by Chen *et al.*,[129] Au@TiO_2 nanoparticles with tunable shell thicknesses were synthesized, demonstrating that the photocatalytic degradation rate of methylene blue was significantly improved—up to five times higher than that of bare Au nanoparticles—highlighting the synergistic effect of the core–shell structure in plasmon-enhanced photocatalysis. This spatial proximity minimizes carrier diffusion distances and eliminates the need for long-range electron transfer through the medium, while also maximizing the reactive surface area of the semiconductor. When these core–shell units are organized into an ordered array, they could potentially function as a plasmonic–photonic crystal wherein each core acts as a plasmonic nanoantenna and the periodic structure induces PBG effects, thereby enhancing light confinement and utilization.

Another multilayer design strategy involves the use of Tamm plasmon–polariton (TPP) structures, which arise at the interface between a thin metallic film and a distributed Bragg reflector, a type of 1D PC.[130,131] This configuration supports a confined

optical mode known as a Tamm plasmon that enables strong field localization at the metal distributed Bragg reflector boundary. When a photocatalytic layer is placed in proximity to this interface, the concentrated optical field can be harnessed to selectively enhance photoactivity at a targeted wavelength. While theoretical proposals and optical demonstrations of such plasmon–photonic "stacks" exist, their practical application in photocatalysis remains at an early stage, with few experimental reports to date.

4.3. Enhancing charge separation and utilization

Besides optimizing light absorption, multifunctional designs aim to improve how photogenerated charges are separated and used in chemical reactions. A key challenge in plasmonic catalysis is that although hot electrons can be transferred from the metal to an adjacent semiconductor, the corresponding hot holes often remain unused and rapidly lose their energy through thermalization. To overcome this limitation, researchers have developed Z-scheme, S-scheme, and dual heterojunction architectures, in which the plasmonic metal functions as a mediator between two semiconductors, facilitating directional charge separation by transferring electrons to one semiconductor and holes to the other.[132,133] Zeng *et al.*[92] designed a TiO_2-based photonic crystal decorated with Au nanoparticles (Au-PMTiNTs), enabling dual-pathway CO_2 photoreduction through either interband transitions or a plasmonic Z-scheme. Similarly, Yang *et al.*[134] reported on a Ag–ZnO inverse opal system in which the deposition of Ag nanoparticles onto the porous ZnO framework creates a junction that facilitates efficient charge transfer. Upon visible light irradiation, Ag nanoparticles absorb light through LSPR and generate energetic electrons. These electrons are injected into the conduction band of ZnO, while the corresponding holes remain in the silver domains. This charge separation reduces electron–hole recombination and increases the availability of reactive carriers for surface redox reactions. The interconnected porous structure of the inverse opal further supports efficient light propagation and reactant diffusion, contributing to the improved photocatalytic performance of the heterojunction system.

In parallel, Xu *et al.*[135] developed an S-scheme Ag/ZnO/CeO_2 inverse opal structure, where the PC enhances light trapping and the plasmonic Ag nanoparticles promote charge separation. This composite achieved a RhB degradation efficiency of 95% after 60 minutes, nearly 2.7 times higher than that of pure ZnO IO, supported by an improved photocurrent response and lower interfacial resistance. Together, these studies highlight how integrating plasmonic nanoparticles within photonic or inverse opal frameworks, combined with Z-scheme or S-scheme charge separation architectures, can enhance solar-driven photocatalysis. Both systems demonstrate that coupling photonic band effects with plasmonic and interfacial charge dynamics enables high activity and selectivity under visible light, advancing multifunctional catalyst design for CO_2 reduction and organic pollutant degradation.

An additional critical design consideration involves the strategic placement of co-catalysts to facilitate multi-electron redox reactions. This approach is demonstrated in the work by Zhao *et al.*,[47] where a 3D ordered macroporous TiO_2–Au–CdS (3DOM TAC) structure was constructed, with TiO_2 serving as the scaffold, CdS as the visible light absorber, and Au nanoparticles as the electron mediator. The system exhibited a hydrogen evolution rate of 3.50 mmol h^{-1} g^{-1} under visible light, driven by the synergistic effects of blue-edge slow photon enhancement and spatially resolved charge transfer. Similarly, in the Ag–Pt–TiO_2 photonic structure developed by Stępnik *et al.*,[136] the bimetallic configuration allowed Pt to accumulate holes for oxidation while Ag facilitated electron transport, supporting multi-electron processes with improved efficiency. These findings highlight that rational placement of co-catalysts within photonic and plasmonic frameworks is essential for maximizing charge utilization in complex solar-driven reactions.

Recent studies have demonstrated that coupling plasmonic resonances with guided photonic modes can significantly enhance charge separation by suppressing radiative losses and promoting hot-carrier generation. Sarkar *et al.*[137] reported large-area metallic and colloidal photonic crystal slabs (mPhCs and cPhCs) that support hybrid waveguide-plasmon modes, enabling polarization and wavelength selective hot-electron injection into TiO_2 waveguides. Enhanced photocurrent responses and ultrafast transient measurements confirmed efficient charge separation under hybrid mode excitation, although the presence of insulating ligands in cPhCs limited charge transfer efficiency. Building on this, Gupta *et al.*[138] employed nanoimprint lithography to assemble monodisperse gold nanoparticle chains directly on TiO_2, eliminating residual resist layers and improving metal–semiconductor contact. Their waveguide-plasmon–polariton (WPP) devices exhibited narrow resonance linewidths (~10 nm), a 7-fold increase in photocurrent under visible-light excitation and effective photocatalytic dye degradation, illustrating the role of hybrid mode engineering and clean interface design in enhancing charge utilization. Together, these studies underscore the potential of 1D plasmonic–photonic crystal architectures as a versatile platform for enhancing charge separation, where tailored hybrid modes enable efficient hot-carrier injection and improved photocatalytic performance.

4.4. Notable recent developments

Several recent advances in plasmonic PC design illustrate how the synergistic integration of light management strategies is translating into notable performance enhancements across photocatalytic applications. One of the most striking demonstrations is the report involving a silica inverse opal embedded with silver nanoparticles, which achieved an extraordinary hydrogen evolution rate of 560 mmol h^{-1} g^{-1}.[45] Unlike typical systems that rely on a semiconductor photoabsorber, this design exploited a purely plasmonic pathway for photocatalysis. The dielectric SiO_2 scaffold was optically transparent and chemically inert, serving solely to confine and amplify incident light through photonic bandgap effects. The resulting enhancement in local electromagnetic fields at the Ag nanoparticle surfaces enabled direct plasmon-induced water splitting, without any contribution from a traditional

semiconductor or the need for an additional Pt co-catalyst. This work underscores the feasibility of efficient "plasmonic-only" catalysis when the optical architecture is precisely optimized.

In another innovative approach, Torras and co-workers[50] demonstrated the fabrication of 2D PC photocatalysts using soft nanoimprint lithography on mesoporous TiO_2 films, subsequently decorated *in situ* with Au nanoparticles. By tailoring the photonic lattice periodicity to match the plasmonic resonance of Au, the team significantly boosted visible-light absorption in the catalyst. Their best-performing configuration achieved a H_2 evolution rate of 8.5 mmol h^{-1} g^{-1} under simulated solar illumination outperforming non-photonic Au–TiO_2 reference systems. Importantly, the use of scalable soft lithography positions this method as a promising route for practical plasmonic–photonic crystal-based device manufacturing.

Addressing the long-standing issue of plasmonic nanoparticle stability, particularly with Ag in aqueous and oxidative environments, recent work has explored protective encapsulation strategies. For example, Ag nanoparticles have been coated with ultra-thin conformal layers of TiO_2 or SiO_2 often *via* ALD to shield them from environmental degradation without impairing their optical properties.[129] These nanometric shells are thin enough (<5 nm) to maintain strong plasmon light coupling while providing a barrier against leaching and oxidation. In plasmonic–photonic crystal architectures, such encapsulation must be carefully controlled to preserve photonic order and avoid pore occlusion; however when successfully implemented, this approach offers a practical path toward long-term photocatalyst durability.

These recent advancements represent a transition from early-generation plasmonic–photonic crystal systems typically based on Au-decorated TiO_2 inverse opals toward more sophisticated architectures that incorporate multiple optical, chemical, and electronic effects. Contemporary plasmonic PCs now exhibit sophisticated optical, structural, and chemical designs that achieve enhanced light harvesting, tunable selectivity, and improved robustness, which are all necessary attributes to extend this emerging class of photocatalysts to a broader range of photocatalytic applications. Many of these designs have demonstrated reaction rate enhancements by factors of two to ten compared to their non-photonic or non-plasmonic counterparts, reflecting the growing maturity of the field. In the following sections, we examine how such innovations have been applied to important energy photocatalysis, including water splitting, hydrogen evolution reaction (HER), and carbon dioxide reduction.

5. Applications in energy photocatalysis

Having established their effective light management properties, it is clear that plasmonic–photonic crystal photocatalysts are highly promising for driving efficient solar-to-chemical energy conversion. In this section, we focus on three interrelated applications: (i) solar water splitting (to concurrently generate hydrogen fuel and oxygen), photocatalytic hydrogen generation (often considered as the half-reaction of water splitting, whereby H_2 is produced with the use of hole scavengers), and carbon dioxide reduction (to produce carbon-based solar fuels). A summary of representative plasmonic–photonic crystal systems, including their fabrication methods, targeted applications, and key performance outcomes, is provided in Table 1 to contextualize and support the following discussion. These applications demand efficient use of visible light and effective management of charge carriers to drive multi-electron chemistry. We highlight representative studies where plasmonic PCs have demonstrated improved performance, and discuss the mechanisms by which they contribute to these energy conversion processes.

5.1. Solar water splitting (H_2 and O_2 generation)

Complete water splitting ($2H_2O \rightarrow 2H_2 + O_2$) is a holy grail reaction in photocatalysis for sustainable energy, producing clean hydrogen fuel from water using sunlight. It is also one of the most demanding reactions, requiring the coordination of two half-reactions (hydrogen evolution and oxygen evolution), each needing multiple electrons and usually requiring co-catalysts for efficiency. Most semiconductor photocatalysts (*e.g.*, bare TiO_2) can only utilize UV light for this reaction, so integrating visible-light plasmonic enhancement is highly attractive.[7–9]

Plasmonic PCs have been applied in both suspended photocatalyst systems and photoelectrochemical (PEC) cells for water splitting. In early work, Zhang *et al.*[48] created a TiO_2 nanotube photonic crystal photoanode seamlessly coupled with Au nanocrystals (Fig. 10A–C) Under visible light (λ > 420 nm), this Au/TiO_2 photonic crystal photoelectrode achieved a photocurrent of ~150 μA cm^{-2}, representing one of the remarkable performances for an Au-sensitized TiO_2 system (Fig. 10D–I). This enhancement was attributed to the Bragg reflection effect of the photonic crystal, which amplified the local light intensity at wavelengths resonant with the plasmonic response of gold (~556 nm), thereby facilitating more efficient hot electron injection into the TiO_2 conduction band. In comparison, analogous gold nanoparticles deposited on a non-photonic TiO_2 nanotube array exhibited much lower photocurrent. These findings demonstrate that slow photon-induced light trapping within photonic architectures can effectively enhance visible-light-driven water splitting activity.

The study by Zhang *et al.*[79] presents a compelling example of how photonic and plasmonic enhancements can be synergistically combined within a $BiVO_4$-based photoanode to achieve efficient water splitting. By structuring Mo-doped $BiVO_4$ into an inverse opal photonic crystal and incorporating Au nanoparticles, they achieved strong coupling between the photonic Bragg resonance and the LSPR of Au, leading to drastic improvements in light harvesting and charge separation. The optimized architecture showed a photocurrent density of 3.1 ± 0.1 mA cm^{-2} at 1.23 V *vs.* RHE under AM 1.5 illumination, which is four times higher than that of the equivalent planar $BiVO_4$ photoanode. The enhancement was most pronounced when the photonic stopband (~513 nm) matched the plasmon

Table 1 Summary of the representative photonic crystal (PC) and plasmonic–photonic crystal (PPC) systems, their fabrication strategies, targeted photocatalytic applications, and key performance outcomes[a]

PC/PPC	Fabrication methods	Applications	Findings	References
1D TiO_2 photonic crystal	Anodization for PCs	Photoelectrochemical water splitting	Enhanced photocurrent due to the slow photon effect	36
3D Au-NP@IOT	Core–shell opal template	Photocatalytic oxidation of acetic acid	Enhanced photoreaction rate due to overlapping of slow photons, LSPR and irradiation source wavelengths	44
3D Ag/SiO_2 opal	Opal template for PCs; infiltration of AgNPs	Photocatalytic hydrogen evolution	Remarkable hydrogen evolution reaction rate of 560 mmol h^{-1} g_{Ag}^{-1} due to overlapping slow photons and the LSPR effect	45
1D Au/TiO_2 nanotube	Anodization for PCs; *in situ* photodeposition of Au	Photoelectrochemical water splitting	High photocurrent density ($\sim$150 μA cm^{-2}) due to synergistic effect of plasmonic absorption and photonic resonances	48
2D TiO_2 PC with Au NPs	Nanoimprint lithography for PCs; microwave Au growth	Photocatalytic hydrogen evolution	Improved activity due plasmonic absorption and photonic resonances	50
3D Au/ZnO-PC	Opal template for PCs; magnetron sputtering of Au	Photodegradation of rhodamine B dye	Enhanced activity due to the synergistic effect of plasmonic absorption and photonic resonances	51
3D TiO_2-IO Au, Ag, Au/AgNP film	Opal template for PCs; metal nanoparticle immersion	Photodegradation and mineralization of acetylene	Enhanced activity due to hot electron transfer from metal nanoparticles	71
3D TiO_2 PC/Au NPs	Opal template for PCs; *in situ* hydrothermal reduction	Photodegradation of 2,4-dichlorophenol	Enhanced photodegradation due to overlapping of slow photons and the LSPR effect	78
3D io-Mo:$BiVO_4$/AuNP	Opal template for PCs; infiltration of AuNPs	Photoelectrochemical water splitting	High photocurrent density ($\sim$3.1 mA cm^{-2}) due to the synergistic effect of plasmonic absorption and photonic resonances	79
3D TiO_2 NP-IO	Opal template	Photodegradation of methylene blue	Enhanced activity	86
3D ATIO	Opal template for PCs; facile wet chemical route	Photodegradation of methylene blue	Enhanced activity due to the synergistic effect of plasmonic and photonic structures	101
3D i-Pt-TiO_2-o	Opal template for PCs; *in situ* photodeposition of Pt	Photodegradation of acid orange	Enhanced photodegradation rate due to synergistic photochemical amplification in the photonic structure	105
1D Cu/TNAs	Anodization for PCs; pulsed electrodeposition	Photocatalytic hydrogen evolution	Enhanced activity due to the LSPR effect	117
3D Pt_x/PC-TiO_2	Opal template for PCs; gas bubbling-assisted membrane reduction of Pt	Photoreduction of CO_2	Enhanced formation of CH_4, H_2, and CO due to the synergistic effect of plasmonic and photonic structures	120
Au@Ag core–shell NPs coupled with a 1D PC slab	Nanoimprint lithography for PCs; colloidal synthesis and drop casting of Au@Ag NPs	Hot-electron photocatalytic reduction of 4-nitrothiolphenol (4-NTP) to 4-aminothiophenol (4-ATP)	Full 4-NTP conversion in 5 min at low power (1.6 mW) due to electronic effects generated by plasmon–photonic hybridization	144

[a] Abbreviations: (1) NP-IO – TiO_2 nanoparticles-inverse opal; ATIO – TiO_2 inverse opal films loaded with silver nanoparticles; (2) Cu/TNAs – Cu nanoparticles deposited on the TiO_2 nanotube arrays; (3) io-Mo:$BiVO_4$/AuNP – Au NPs infiltrated Mo-doped $BiVO_4$ inverse opal; (4) i-Pt-TiO_2-o – Pt loaded on the TiO_2 inverse opal; (5) 3D Au-NP@IOT – titania inverse opal photonic crystals with a single gold nanoparticle in each void.

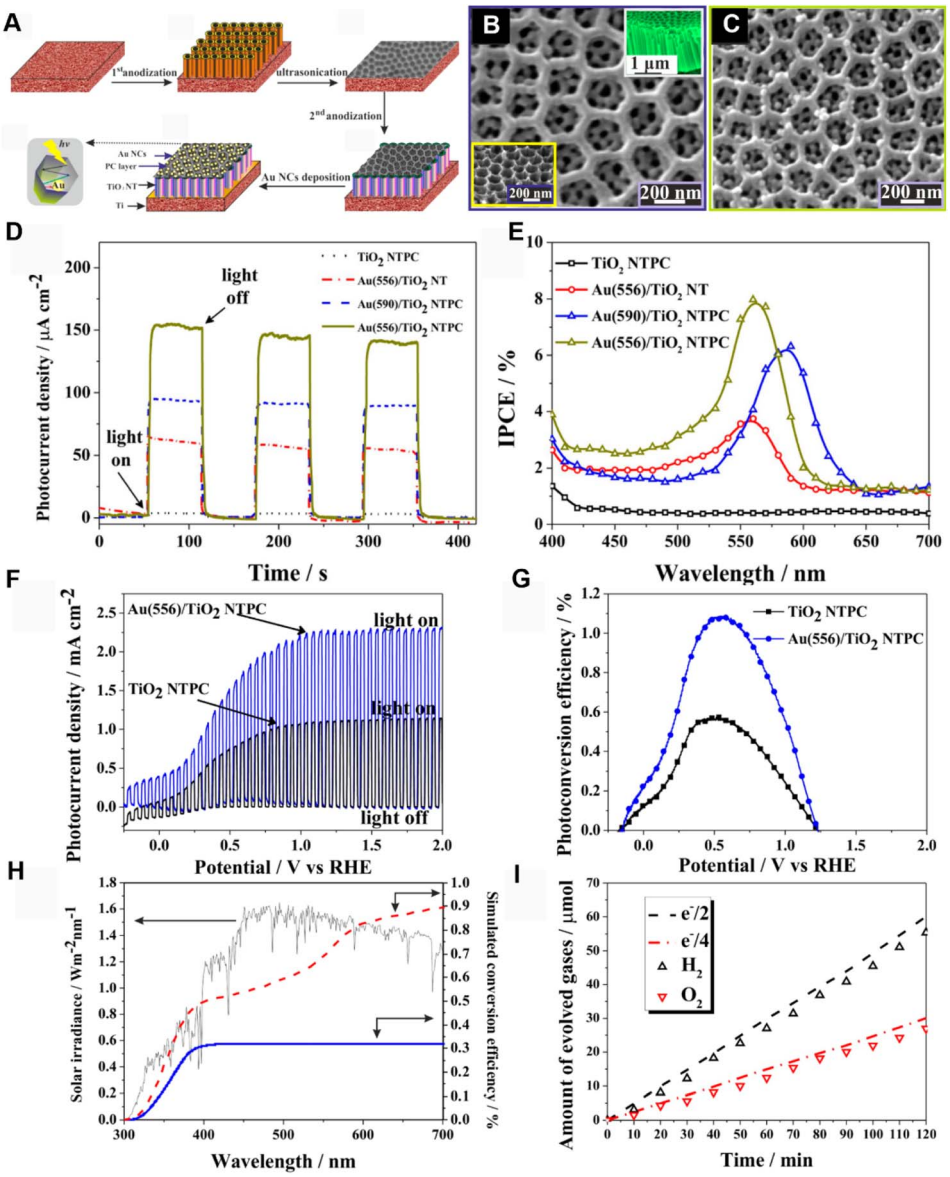

Fig. 10 (A) Schematic diagram of the Au/TiO_2 nanotube photonic crystal fabrication procedure. SEM images of (B) TiO_2 nanotube photonic crystals and (C) Au/TiO_2 nanotube photonic crystals. (D) Amperometric *I*–*t* curves at an applied potential of 1.23 V *vs.* RHE under illumination of visible light with wavelength ≥420 nm with 60 s light on/off cycles. (E) IPCE plots in the range of 400–700 nm at 1.23 V *vs.* RHE. (F) Photoelectrochemical performance of various TiO_2-based platforms. Linear sweep voltammograms recorded under chopped illumination at a scan rate of 5 mV s^{-1}. (G) Photoconversion efficiency plotted as a function of applied potential. (H) Wavelength-dependent photoconversion efficiencies of Au(556)/TiO_2 nanotube photonic crystals and TiO_2 nanotube photonic crystals, obtained by integrating the IPCE spectra at 0.5 V *vs.* RHE with the AM 1.5G standard solar spectrum (ASTM G-173-03). (I) Time-dependent gas evolution for the Au(556)/TiO_2 nanotube photonic crystal electrode under simulated solar irradiation at 0.5 V *vs.* RHE. Reproduced with permission from ref. 48. Copyright 2012 American Chemical Society.

resonance of Au and the $BiVO_4$ absorption edge, highlighting the critical importance of spectral alignment. Furthermore, gas evolution measurements confirmed stoichiometric H_2 and O_2 production with faradaic efficiencies exceeding 95%, demonstrating true overall water splitting driven by this plasmonic–photonic nanostructure.

Achieving true overall water splitting using plasmonic PCs remains a formidable challenge, primarily due to the need for balanced and efficient execution of both the hydrogen and oxygen evolution half-reactions. One promising approach is the implementation of a Z-scheme system, wherein a plasmonic photocatalyst optimized for hydrogen generation is coupled with a separate photoanode tailored for oxygen evolution, allowing each half-reaction to be driven independently by light. Within such tandem architectures, plasmonic PCs can enhance the hydrogen evolution side by amplifying light absorption through slow photon effects and LSPR, thereby improving hot carrier generation, charge separation, and catalytic efficiency.[139] For instance, one could pair an Au/TiO_2 photonic crystal (H_2 evolution under visible light irradiation) with a $BiVO_4$

photoanode (O_2 evolution under visible light irradiation) in a two-component system with a redox mediator. Although this approach enters the photoelectrochemical domain, conceptually the enhanced H_2 generation rate from the plasmonic PC would help balance the O_2 evolution.

Several studies have demonstrated that plasmonic metals on TiO_2 can enable overall water splitting under visible light by enhancing light absorption and charge separation. Tanaka *et al.*[140] showed that combining plasmonic Au with TiO_2 and a Ni co-catalyst produced H_2 and O_2 in a stoichiometric 2 : 1 ratio under visible irradiation. Qin *et al.*[119] reported a hierarchical TiO_2 structure decorated with large Pt nanoparticles, which exhibited broad plasmonic absorption and superior overall water splitting performance due to the dual benefits of a strong Schottky barrier and Pt's catalytic activity. Similarly, Melvin *et al.*[141] also observed that a bimetallic Au–Pt system on TiO_2 could drive overall splitting with a quantum yield of ~0.8% under sunlight without sacrificial agents. These findings highlight the effectiveness of plasmon-enhanced TiO_2 systems for solar H_2 production from water and suggest that incorporating such plasmonic–catalytic configurations into photonic crystal frameworks could further amplify light harvesting and improve reaction efficiency.

Plasmonic PCs represent a promising approach to overcome a major limitation in solar water splitting by improving visible light utilization. These systems combine bandgap excitation, which drives charge generation under UV light, with plasmonic excitation that extends absorption into the visible range, resulting in a more continuous solar response. Studies have reported improvements of two- to five-fold in hydrogen or oxygen evolution rates, highlighting the effectiveness of coupling photonic light trapping with plasmon-induced charge transfer.[48,79] These gains are particularly meaningful given the complexity of water splitting, which involves multiple charge carriers and catalytic steps. As research progresses toward enhancing structural stability and integrating robust co-catalysts, plasmonic PCs are poised to play a central role in efficient and scalable solar water splitting technologies.

5.2. Photocatalytic hydrogen generation (H_2 evolution)

In practice, many studies examine the hydrogen generation half-reaction separately. Photocatalytic hydrogen generation usually refers to the light-driven H_2 evolution half-reaction, often studied using a sacrificial hole scavenger (such as methanol, ethanol, or Na_2S/Na_2SO_3) to provide electrons and circumvent the need for O_2 evolution. It essentially provides a metric of how effectively a catalyst can reduce protons to H_2 under light. Plasmonic PCs have achieved some of the highest H_2 evolution rates reported for particulate-based photocatalysis.

A notable example is the Ag/SiO_2 opal system that achieved 560 mmol per h per g H_2 with only Ag as the active material.[45] For comparison, even the best conventional photocatalysts (like Pt/TiO_2 with concurrent UV and visible light irradiation) typically produce H_2 on the order of a few mmol h^{-1} g^{-1} under similar conditions (Fig. 11). The observed enhancement of over 10^6 times compared to bare Ag nanoparticles indicates that Ag nanoparticles alone exhibit negligible catalytic activity for water splitting, which is consistent with their known limitations. Notably, when embedded within a photonic crystal, the Ag nanoparticles become highly active likely due to strong field localization or multiphoton excitation effects enabled by the photonic structure. This finding opens up the intriguing possibility of achieving plasmon-driven hydrogen generation without relying on a semiconductor, where energetic hot electrons from Ag could directly reduce protons to H_2. The oxidation half-reaction is sustained by methanol serving as a hole scavenger. It is also noteworthy that the Ag/SiO_2 opal platform operated without the need for an additional co-catalyst, suggesting that the Ag surface alone was sufficient to facilitate both redox processes within the photonic environment.

Similarly, Au-decorated TiO_2 2D PCs have shown substantial enhancement in hydrogen production under UV and visible light due to combined photonic and plasmonic effects.[50] The designed Au/TiO_2 2D photonic crystal produced up to 8.5 mmol per h per g H_2 under full solar spectrum illumination using a methanol–water mixture as a sacrificial electron donor. This performance corresponded to a 28-fold increase over bare TiO_2 and up to a 62% enhancement compared to non-patterned flat substrates. The improvement was attributed to the synergistic effects of photonic light trapping from the 600 nm periodic grating and efficient plasmonic excitation of gold nanoparticles, which extended light harvesting well into the visible range beyond the intrinsic UV response of TiO_2.

In contrast to these semiconductor-based PPC systems, a complementary strategy was demonstrated using purely plasmonic architectures that mimic photonic crystal behavior through periodic nanoparticle ordering. A notable example is a 2D bimetallic plasmonic supercrystal composed of hexagonally packed Au nanoparticles with Pt catalytic sites positioned in the interparticle gaps.[142] This system supports SLRs that generate intense localized near-fields, directly activating Pt sites for visible-light-driven hydrogen evolution *via* formic acid dehydrogenation. Remarkably, the catalyst achieved H_2 production rates over 130 mmol h^{-1} g^{-1} under solar irradiance level illumination without relying on a semiconductor or co-catalyst support. These findings suggest a promising pathway for future plasmonic photocatalyst designs, where rational nanoparticle arrangement and plasmon–plasmon coupling can replicate key functionalities of photonic crystals and enable efficient solar-to-hydrogen conversion in minimal or all metallic platforms.

It is worth mentioning that there is a growing interest in exploring infrared-driven hydrogen generation, an area typically overlooked since infrared light is commonly dissipated as heat in photocatalysis. However, incorporating plasmonic nanostructures such as copper or heavily doped metal oxide nanoparticles enables photoabsorption in the infrared region and opens the possibility of harnessing this spectral range through photothermal or multiphoton mechanisms. Designing PCs with larger periodicities (on the order of 1–2 micrometers) could enable effective infrared light trapping within catalyst platforms, enhancing localized heating when combined with IR-absorbing plasmonic elements. While still speculative, such

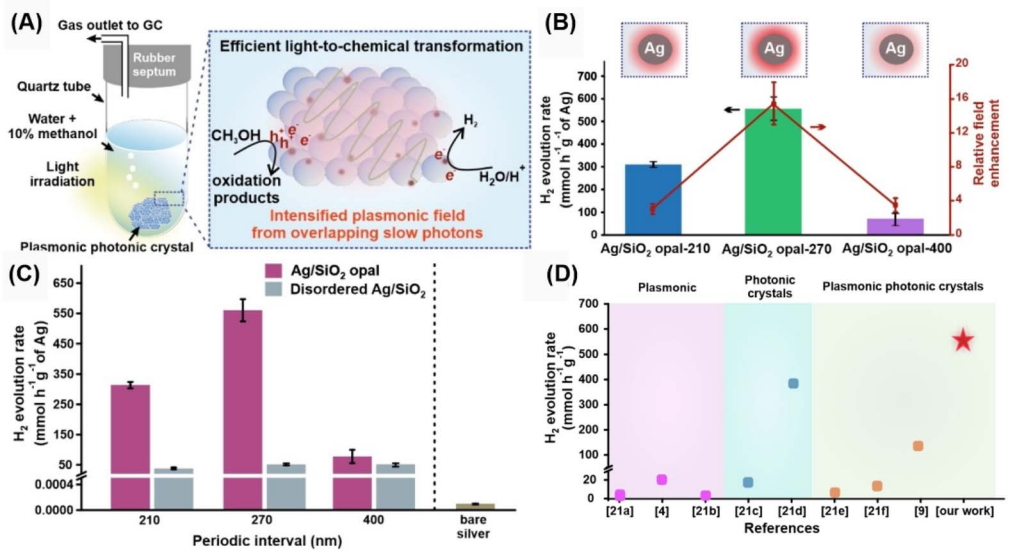

Fig. 11 (A) Schematic illustration of the photoreactor setup using the Ag/SiO_2 opal as plasmonic catalysts for the HER. (B) HER and the relative field enhancement observed from various plasmonic PCs with different opal diameters. The inset depicts electromagnetic field strength observed for various plasmonic–photonic catalysts. (C) H_2 evolution rate from water in the presence of Ag/SiO_2 opals, disordered Ag/SiO_2 platforms, or bare Ag nanoparticles under light irradiation. (D) Comparison of photocatalytic H_2 production rates between the optimized plasmonic–photonic catalytic architecture and other emerging photocatalyst designs incorporating PCs, hybrid plasmonic–semiconductor systems, and plasmonic–photonic ensembles under ambient conditions. Reproduced with permission from ref. 45. Copyright 2024 Wiley.

an approach could convert infrared energy into useable thermal gradients to drive thermocatalytic H_2 production, as demonstrated in studies which employed Au nanoparticles and carbon quantum dot-loaded TiO_2 nanotube arrays as photocatalysts.[143] PCs offer a tunable platform that can be adapted not only for visible light harvesting but also for managing infrared radiation, suggesting their potential as a framework for integrated solar–thermal catalytic microreactors.

Collectively, plasmonic PCs offer a powerful strategy for enhancing solar-driven hydrogen evolution by extending light absorption well beyond the ultraviolet. These hybrid materials simultaneously harvest UV photons through semiconductor bandgap excitation and capture visible light *via* plasmonic resonance, with additional contributions from localized photothermal effects. Their interconnected porous architectures also facilitate rapid gas diffusion, which supports efficient hydrogen evolution kinetics. Recent systems based on plasmonic PCs are beginning to achieve hydrogen production rates comparable to those of noble-metal-assisted photocatalysts operating under UV light, yet they do so primarily under visible irradiation, marking a significant advance in solar energy utilization. Moving forward, performance could be further improved by integrating multiple plasmonic metals to broaden the spectral response, or by coupling plasmonic PCs with tandem photovoltaic cells to introduce an internal bias, paving the way toward practical and scalable solar-to-hydrogen conversion technologies.

5.3. CO_2 reduction to solar fuels

Photocatalytic carbon dioxide reduction seeks to convert CO_2, a chemically stable linear molecule, into useful fuels such as carbon monoxide, methane, or methanol using solar energy mimicking natural photosynthesis. This reaction presents challenges often exceeding those of water splitting, as it requires multiple proton electron transfers and involves competing reaction pathways leading to diverse products.[3,5] Another persistent challenge in CO_2 photoreduction is the limited diffusion of CO_2 molecules to active catalytic sites, which hampers reaction efficiency.[3] PCs, particularly inverse opal structures, offer a solution by providing a highly porous and interconnected network that facilitates gas diffusion and extends the optical path length through multiple light scattering events. This architecture not only enhances CO_2 accessibility but also improves light absorption *via* the slow photon effect, thereby increasing the generation of charge carriers necessary for the reduction process. Incorporating photonic and plasmonic enhancements is particularly advantageous in this context, as they can intensify light absorption, promote charge separation, overcome mass transport limitations, and improve both the conversion efficiency and selectivity under solar irradiation.

A plasmonic–photonic catalyst composed of Au-decorated periodically modulated TiO_2 nanotube arrays demonstrates high efficiency and tunable selectivity in photocatalytic CO_2 reduction. The plasmonic–photonic crystal architecture achieves high-rate CO_2 photoreduction with wavelength-controlled product selectivity.[92] Under full-spectrum solar irradiation, the photocatalytic platform preferentially produces methane at a rate of 302 $\mu mol\ g^{-1}\ h^{-1}$ with 89.3% selectivity. When exposed to visible light ($\lambda > 420$ nm) followed by solar light, the reaction shifts to generate formaldehyde (420 $\mu mol\ g^{-1}\ h^{-1}$) and carbon monoxide (323 $\mu mol\ g^{-1}\ h^{-1}$), indicating operation *via* a plasmonic Z-scheme pathway. This optical modulation arises from the interplay between photonic bandgap effects and localized

surface plasmon resonance in Au, enabling control over charge carrier dynamics and reaction pathways. The results highlight how photonic crystal architectures can be strategically tailored to tune the energetics and selectivity of the plasmon-enhanced CO_2 reduction reaction.

Jiao *et al.*[120] employed TiO_2 PCs decorated with uniformly distributed platinum nanoparticles, synthesized *via* a gas bubbling-assisted membrane reduction method. This architecture enhanced light harvesting through the slow photon effect, which increased the residence time of photons near the TiO_2 absorption edge, thereby boosting the generation of electron–hole pairs. The embedded Pt nanoparticles served as electron sinks and catalytic sites, promoting spatial charge separation and lowering the activation barrier for CO_2 reduction. Mechanistically, photogenerated electrons were efficiently transferred from the TiO_2 conduction band to the Pt surface, where they facilitated the multi-electron reduction of CO_2 to methane, while holes in TiO_2 oxidized water to provide the necessary protons. The resulting Pt/PC-TiO_2 catalyst achieved a CH_4 production of 2.416 mmol over 450 minutes, approximately 2.4 times higher than that of undoped photonic TiO_2, demonstrating its effectiveness in selective CO_2 reduction in aqueous media.

For instance, plasmonic–photonic crystal systems have exhibited enhancements in CH_4 production, achieving yields several orders of magnitude higher than those observed with unstructured TiO_2 owing to their ability to engineer light–matter interactions at the nanoscale.[53] These structures enable better control over reaction pathways by tailoring the spatial and spectral distribution of light within the catalyst as CO_2 reduction requires a specific energetic threshold ($\sim$2.3 eV for CO formation) and coupling UV-induced semiconductor excitation with visible-light plasmonic effects facilitates complex multi-electron transfer processes. The photonic crystal framework enhances light trapping through the slow photon effect, while plasmonic components generate hot carriers or localized heating to activate CO_2 more efficiently. This synergy helps address the long-standing challenge of low selectivity in CO_2 photoreduction by allowing spatially and spectrally resolved activation of different intermediates. While the field is still evolving, such hybrid catalysts are poised to play a central role in future light-driven CO_2-to-fuel technologies, especially when paired with co-catalysts designed to promote specific reaction pathways and target product generation.

6. Conclusion and outlook

Plasmonic–photonic photocatalysts have emerged as a promising class of hybrid materials capable of addressing critical limitations in conventional photocatalysis. By combining the long-range light-trapping ability of PCs with the intense localized field enhancement and hot charge carrier generation offered by plasmonic nanostructures, these hybrid systems achieve markedly improved light absorption, broadened spectral utilization extending into the visible and near-infrared regions, and enhanced charge separation. Such synergistic optical and electronic enhancements have led to notable performance gains in solar-driven photocatalytic reactions. Recent progress in nanomaterial synthesis, structural engineering, and hierarchical integration has further advanced plasmonic PCs as pivotal platforms for energy photocatalysis. Notably, these materials have demonstrated the ability to efficiently facilitate hydrogen evolution from water, carbon dioxide conversion to value-added fuels, and other reactions central to green energy technologies, particularly under visible light where traditional wide-band gap semiconductors are often ineffective. The precise tunability of their photonic and plasmonic elements enables optimized spectral matching and coupling, allowing plasmonic PCs to achieve catalytic efficiencies that approach or even surpass those of conventional systems that depend on ultraviolet excitation and extensive use of expensive noble-metal co-catalysts.

Despite these advancements, several critical challenges must be overcome to fully realize the potential of plasmonic–photonic crystal photocatalysts in practical applications. Achieving long-term photostability remains a key hurdle, as prolonged illumination, environmental exposure, and operational stress can degrade both photonic structures and plasmonic elements. Equally important is the ability to reproduce these complex architectures consistently across large areas and at industrial scales, which is often hindered by fabrication variability and structural defects. Furthermore, the widespread deployment of these materials depends on the development of photocatalysts that are both environmentally sustainable and economically viable, reducing reliance on scarce or toxic elements. Addressing these issues will require continued interdisciplinary research, particularly to deepen our understanding of interfacial charge dynamics and to optimize the interaction among plasmonic nanostructures, photonic architectures, and semiconductor components. Mastering this triadic coupling is essential for enhancing charge transfer efficiency and maximizing light-to-chemical transformation while maintaining structural integrity under realistic operating conditions.

To guide future progress, we propose several key outlooks that build on the integrated design principles of plasmonic–photonic crystal photocatalysts. One promising direction lies in developing more effective light management strategies that synergistically combine photonic crystal architectures with plasmonic nanostructures. PCs offer spatial and spectral control over light propagation, while plasmonic elements provide intense localized field enhancement and generate energetic charge carriers. Together, these features enable more comprehensive photon harvesting across the solar spectrum. Embedding such hybrid materials into advanced reactor platforms, such as microreactors or photoreactors equipped with reflective surfaces or light-recycling systems, can further optimize photon distribution and utilization. In these configurations, photonic structures may act as spectral filters or light-guiding layers that direct specific wavelength bands toward customized catalytic domains. Meanwhile, the integration of thermally robust plasmonic materials enables hybrid photochemical and photothermal processes that utilize both visible and infrared components of sunlight. These design

complexities increasingly rely on computational modeling, including photonic simulations coupled with reactor geometries, to optimize light–matter interactions. Concurrently, advances in nanofabrication have now made it possible to engineer photonic structures with graded refractive indices, resonant cavities, or deliberate defect sites that enhance light localization. When coupled with tailored plasmonic nanoparticle arrangements, these innovations unlock new catalytic capabilities, from site-selective molecular transformations to high-efficiency operation under diffuse light conditions.

A central challenge in advancing plasmonic–photonic crystal photocatalysis lies in fully harnessing the additional charge carriers produced through plasmonic excitation. These hot electrons and holes must be directed efficiently into chemical reaction pathways rather than lost through recombination or dissipated as heat. However, the fundamental mechanisms that govern hot carrier generation, transport, and transfer in these hybrid systems are still not fully understood. To address this, advanced spectroscopic tools such as ultrafast transient absorption spectroscopy and spatially resolved photoluminescence mapping are essential, particularly in regions influenced by slow photon effects where light–matter interactions are intensified. In addition to improving charge carrier efficiency, controlling the selectivity of complex multi-electron reactions, such as in carbon dioxide reduction, remains a critical objective. Recent studies indicate that the photonic environment can influence reaction outcomes, with specific illumination wavelengths favoring the production of either methane or carbon monoxide. This observation highlights the potential to tailor reaction pathways by precisely engineering the optical properties of the catalyst.

Although self-assembly techniques for fabricating opal-based PCs offer a cost-effective route, achieving uniform structures over large areas or at industrial scales remains challenging due to issues such as defect control and structural reproducibility. In contrast, top–down lithographic methods like nanoimprint lithography provide greater precision and pattern fidelity but introduce higher manufacturing costs and process complexity. Another major constraint in current plasmonic–photonic crystal designs is the dependence on noble metals such as gold, silver, and platinum. These materials, while highly effective, are expensive and scarce, which limits their sustainability for widespread deployment. Consequently, there is increasing interest in replacing noble metals with earth-abundant alternatives such as copper, aluminum, or conductive metal nitrides. However, these substitutes often suffer from lower plasmonic performance or chemical stability, necessitating additional strategies such as protective coatings or encapsulation layers to preserve functionality. Striking a balance between catalytic performance and economic viability is therefore essential. For example, a composite material using a silver–copper alloy within a polymer-based photonic crystal could potentially serve as a lower-cost alternative to traditional gold–titania systems, provided that similar levels of photocatalytic activity can be maintained.

For real-world applications, the integration of plasmonic–photonic crystal photocatalysts into functional devices remains a critical and necessary step. Ultimately, photocatalytic materials must be configured into practical formats such as panels for hydrogen generation or electrodes for use in PEC cells. However, many photonic crystal-based catalysts are fabricated as powders or delicate freestanding films, making their direct transfer onto solid substrates without structural disruption a long-standing challenge. To overcome this, researchers are investigating more robust support frameworks, including photonic crystal fibers and monolithic scaffolds, which can maintain the structural integrity of the catalyst while operating under realistic environmental conditions. In the domain of solar fuel production *via* flow reactors, embedding these structured catalysts into pellets or foams is emerging as a viable design approach. A particularly promising method is the use of 3D printing, such as direct ink writing, to fabricate photonic lattices from photocatalytic materials like titanium dioxide. These lattices can then be functionalized with plasmonic nanoparticles to enable enhanced light harvesting. This technique offers both structural tunability and scalability. Additionally, modular, multilayered architectures are being explored, in which a top photonic crystal layer selectively manipulates sunlight, enhancing certain wavelengths while allowing others to pass through to the underlying catalytic layers. Such configurations mimic the spectral optimization strategy used in tandem solar cells and represent an innovative path forward for achieving high-efficiency solar-to-chemical energy conversion.

Overall, plasmonic–photonic crystal photocatalysts represent a transformative approach for solar energy conversion, merging advanced light management with efficient catalytic functionality. Their ability to harness a broad spectrum of sunlight and drive key reactions such as hydrogen generation and CO_2 reduction has positioned them at the forefront of energy photocatalysis research. With continued progress in materials design, fabrication, fundamental understanding, and integration, these hybrid systems are poised to overcome current limitations and unlock new possibilities in solar fuel production. The prospects for plasmonic PCs are certainly bright, with their unique capabilities offering a promising pathway toward scalable, sustainable energy technologies.

Conflicts of interest

There are no conflicts to declare.

Data availability

No new data were generated or analysed in this review article. All data and figures are sourced from previously published literature, which are appropriately cited throughout the manuscript. Figures adapted or reproduced from other works are included with permission from the respective publishers.

Acknowledgements

H. K. L. acknowledges the funding support from the Singapore Ministry of Education (AcRF Tier 1 RG92/24), the Agency for Science, Technology and Research (A*STAR, Singapore; MTC

IRG M23M6c0098), and the Nanyang Technological University start-up grants.

References

1 J. Luo, S. Zhang, M. Sun, L. Yang, S. Luo and J. C. Crittenden, *ACS Nano*, 2019, **13**, 9811–9840.
2 A. Chakravorty and S. Roy, *Sustainable Chem. Environ.*, 2024, **8**, 100155.
3 X. Li, J. Yu, M. Jaroniec and X. Chen, *Chem. Rev.*, 2019, **119**, 3962–4179.
4 H. Song, S. Luo, H. Huang, B. Deng and J. Ye, *ACS Energy Lett.*, 2022, **7**, 1043–1065.
5 C. Fu, Z. Wan, X. Yang, J. Zhang and Z. Zhang, *J. Mater. Chem. A*, 2024, **12**, 28618–28657.
6 H. Nishiyama, T. Yamada, M. Nakabayashi, Y. Maehara, M. Yamaguchi, Y. Kuromiya, Y. Nagatsuma, H. Tokudome, S. Akiyama, T. Watanabe, R. Narushima, S. Okunaka, N. Shibata, T. Takata, T. Hisatomi and K. Domen, *Nature*, 2021, **598**, 304–307.
7 K. Nakata and A. Fujishima, *J. Photochem. Photobiol., C*, 2012, **13**, 169–189.
8 T. A. Kandiel, A. Feldhoff, L. Robben, R. Dillert and D. W. Bahnemann, *Chem. Mater.*, 2010, **22**, 2050–2060.
9 K. Wang, M. Janczarek, Z. Wei, T. Raja-Mogan, M. Endo-Kimura, T. M. Khedr, B. Ohtani and E. Kowalska, *Catalysts*, 2019, **9**, 1054.
10 J. Choi, W. Jung, S. Gonzalez-Carrero, J. R. Durrant, H. Cha and T. Park, *Energy Environ. Sci.*, 2024, **17**, 7999–8018.
11 Y. Bai, K. Nakagawa, A. J. Cowan, C. M. Aitchison, Y. Yamaguchi, M. A. Zwijnenburg, A. Kudo, R. S. Sprick and A. I. Cooper, *J. Mater. Chem. A*, 2020, **8**, 16283–16292.
12 R. Shah, D. Khan, A. Al-Anazi, W. Ahmad, I. Ullah, N. S. Shah and J. A. Khan, *Appl. Catal. O: Open*, 2025, **1**, 207043.
13 D. K. Bhat, H. Bantawala and U. S. Shenoy, *Nanoscale Adv.*, 2020, **2**, 5688–5698.
14 C. Han, B. K. Kundu, Y. Liang and Y. Sun, *Adv. Mater.*, 2024, **36**, 2307759.
15 M. Z. Rahman, F. Raziq, H. Zhang and J. Gascon, *Angew. Chem., Int. Ed.*, 2023, **62**, e202305385.
16 M. Z. Qamar, F. K. Asiam, H. C. Kang, R. Shahid, A. K. Kaliamurthy, C. Chen, J. Lim, M. M. Rahman and J.-J. Lee, *Small*, 2025, **21**, 2411853.
17 S. Freeburne, J. L. Sacco, E. W. Gomez and C. W. Pester, *Macromol. Chem. Phys.*, 2023, **224**, 2300283.
18 A. Kumar, P. Choudhary, A. Kumar, P. H. C. Camargo and V. Krishnan, *Small*, 2022, **18**, 2101638.
19 R. Basumatary, D. Konwar and A. Ramchiary, *Sol. Energy Mater. Sol. Cells*, 2025, **282**, 113353.
20 S. Linic, P. Christopher and D. B. Ingram, *Nat. Mater.*, 2011, **10**, 911–921.
21 S. Liu, Z. Wu, Z. Zhu, K. Feng, Y. Zhou, X. Hu, X. Huang, B. Zhang, X. Dong, Y. Ma, K. Nie, J. Shen, Z. Wang, J. He, J. Wang, Y. Ji, B. Yan, Q. Zhang, A. Genest, X. Zhang, C. Li, B. Wu, X. An, G. Rupprechter and L. He, *Nat. Commun.*, 2025, **16**, 2245.
22 S. Tan, A. Argondizzo, J. Ren, L. Liu, J. Zhao and H. Petek, *Nat. Photonics*, 2017, **11**, 806–812.
23 A. J. Bard and M. G. Kraeutler, *J. Am. Chem. Soc.*, 1978, **100**, 4317–4319.
24 T. Bora, D. Zoepfl and J. Dutta, *Sci. Rep.*, 2016, **6**, 26913.
25 S. Luo, X. Ren, H. Lin, H. Song and J. Ye, *Chem. Sci.*, 2021, **12**, 5701–5719.
26 S. Li, J. Yang, X. Ruan, X. Cui and S. K. Ravi, *Adv. Funct. Mater.*, 2025, 2503186.
27 N. H. Abbas, R. Rasuli and P. N. Panahi, *Sci. Rep.*, 2025, **15**, 8207.
28 Y. Liu, C.-H. Liu, T. Debnath, Y. Wang, D. Pohl, L. V. Besteiro, D. M. Meira, S. Huang, F. Yang, B. Rellinghaus, M. Chaker, D. F. Perepichka and D. Ma, *Nat. Commun.*, 2023, **14**, 541.
29 N. M. Ngo, M. D. Nguyen, H.-V. Tran, J. M. Lee and T. R. Lee, *ACS Appl. Energy Mater.*, 2025, **8**, 5378–5387.
30 S. H. Abed, R. A. Madhi, K. Heydaryan and A. F. Shamkhi, *Biomass Convers. Biorefin.*, 2025, **15**, 5631–5641.
31 M. Curti, C. B. Mendive, M. A. Grela and D. W. Bahnemann, *Mater. Res. Bull.*, 2017, **91**, 155–165.
32 Y. Wan, J. Wang, X. Wang, H. Xu, S. Yuan, Q. Zhang and M. Zhang, *Opt. Mater.*, 2019, **96**, 109287.
33 G. L. Chiarello, A. Zuliani, D. Ceresoli, R. Martinazzo and E. Selli, *ACS Catal.*, 2016, **6**, 1345–1353.
34 C. López, *Adv. Mater.*, 2003, **15**, 1679–1704.
35 E. Yablonovitch, *J. Opt. Soc. Am. B*, 1993, **10**, 283–295, DOI: **10.1364/JOSAB.10.000283**.
36 O. Deparis, S. R. Moucheta and B.-L. Su, *Phys. Chem. Chem. Phys.*, 2015, **17**, 30525–30532.
37 Y. Yang, G. Wang, Q. Deng, D. H. L. Ng and H. Zhao, *ACS Appl. Mater. Interfaces*, 2014, **6**, 3008–3015.
38 Z. Zhang and H. Wu, *Chem. Commun.*, 2014, **50**, 14179–14182.
39 S. John, *Phys. Rev. Lett.*, 1987, **58**, 2486–2489.
40 X. Zhang and S. John, *Opt. Express*, 2021, **29**, 22376–22391.
41 S. Saravanan and R. S. Dubey, *Nanosyst.: Phys., Chem., Math.*, 2019, **10**, 63–69.
42 M. Meng, H. Zhou, J. Yang, L. Wang, H. Yuan, Y. Hao and Z. Gan, *Nanomaterials*, 2024, **14**, 1695.
43 T. K. Rahul and N. Sandhyarani, *ChemNanoMat*, 2018, **4**, 642–648.
44 T. Raja-Mogan, A. Lehoux, M. Takashima, E. Kowalska and B. Ohtani, *Chem. Lett.*, 2021, **50**, 711–713.
45 T. Raja Mogan, J. Zhang, L. S. Ng, S. K. Boong, C. Chong, J.-K. Lee, H. Li and H. K. Lee, *Angew. Chem., Int. Ed.*, 2024, **63**, e202401277.
46 S. Y. Lim, C. S. Law, L. Liu, M. Markovic, A. D. Abell and A. Santos, *Catal. Sci. Technol.*, 2019, **9**, 3158–3176.
47 H. Zhao, Z. Hu, J. Liu, Y. Li, M. Wu, G. Van Tendeloo and B.-L. Su, *Nano Energy*, 2018, **47**, 266–274.
48 Z. Zhang, L. Zhang, M. N. Hedhili, H. Zhang and P. Wang, *Nano Lett.*, 2013, **13**, 14–20.
49 S. Sarkar, V. Gupta, M. Kumar, J. Schubert, P. T. Probst, J. Joseph and T. A. F. Konig, *ACS Appl. Mater. Interfaces*, 2019, **11**, 13752–13760.

50 M. Torras, P. Molet, L. Soler, J. Llorca, A. Roig and A. Mihi, *Adv. Energy Mater.*, 2022, **12**, 2103733.
51 S. Meng, D. Li, X. Fu and X. Fu, *J. Mater. Chem. A*, 2015, **3**, 23501–23508.
52 X. Wang, X. Li and J. Low, *RSC Adv.*, 2021, **11**, 8751–8758.
53 Y. Wei, J. Jiao, Z. Zhao, J. Liu, J. Li, G. Jiang, Y. Wang and A. Duan, *Appl. Catal., B*, 2015, **179**, 422–432.
54 F. Y. Alzoubi, A. A. Ahmad, I. A. Aljarrah, A. B. Migdadi and Q. M. Al-Bataineh, *J. Mater. Sci.: Mater. Electron.*, 2023, **34**, 2128.
55 X. Fan, W. Zheng and D. J. Singh, *Light: Sci. Appl.*, 2014, **3**, e179.
56 C. Dab, T. Reji and R. Andreas, *RSC Adv.*, 2018, **8**, 19616–19626.
57 C. Awada, C. Dab, M. G. Grimaldi, A. Alshoaibi and F. Ruffino, *Sci. Rep.*, 2021, **11**, 4714.
58 M. G. Méndez-Medrano, E. Kowalska, A. Lehoux, A. Herissan, B. Ohtani, S. Rau, C. Colbeau-Justin, J. L. Rodríguez-Lo&pacute;ez and H. Remita, *J. Phys. Chem. C*, 2016, **120**, 25010–25022.
59 H. Chen, X. Kou, Z. Yang, W. Ni and J. Wang, *Langmuir*, 2008, **24**, 5233–5237.
60 S. Linic, P. Christopher and D. B. Ingram, *Nat. Mater.*, 2011, **10**, 911–921.
61 L. Zhou, Q. Huang and Y. Xia, *Chem. Rev.*, 2024, **124**, 8597–8619.
62 L. V. Besteiro, X.-T. Kong, Z. Wang, G. Hartland and A. O. Govorov, *ACS Photonics*, 2017, **4**, 2759–2781.
63 S. Bouhadoun, C. Guillard, F. Dappozze, S. Singh, D. Amans, J. Bouclée and N. Herlin-Boime, *Appl. Catal., B*, 2015, **174–175**, 367–375.
64 M. Xiao, R. Jiang, F. Wang, C. Fang, J. Wang and J. C. Yu, *J. Mater. Chem. A*, 2013, **1**, 5790–5805.
65 Z. Liu, W. Hou, P. Pavaskar, M. Aykol and S. B. Cronin, *Nano Lett.*, 2011, **11**, 1111–1116.
66 X. Chen, H.-Y. Zhu, J.-C. Zhao, Z.-F. Zheng and X.-P. Gao, *Angew. Chem., Int. Ed.*, 2008, **47**, 5353–5356.
67 Y. Shiraishi, N. Yasumoto, J. Imai, H. Sakamoto, S. Tanaka, S. Ichikawa, B. Ohtani and T. Hirai, *Nanoscale*, 2017, **9**, 8349–8361.
68 S. Veziroglu, J. Shondo, T. Tjardts, T. B. Sarwar, A. Sünbül, Y. K. Mishra, F. Faupel and O. C. Aktas, *Nanoscale Adv.*, 2024, **6**, 6096–6108.
69 V. Jovic, H. Idriss and G. I. N. Waterhouse, *Chem. Phys.*, 2016, **479**, 109–121.
70 D. A. Corella and B. Baruah, *RSC Adv.*, 2017, **7**, 47038–47048.
71 F. Temerov, B. Ankudze and J. J. Saarinen, *Mater. Chem. Phys.*, 2020, **242**, 122471.
72 Y. Zhang, K. Li, F. Su, Z. Cai, J. Liu, X. Wu, H. He, Z. Yin, L. Wang, B. Wang, Y. Tian, D. Luo, X. W. Sun and Y. J. Liu, *Opt. Express*, 2019, **27**, 15391–15404.
73 G. L. Chiarello, A. Zuliani, D. Ceresoli, R. Martinazzo and E. Selli, *ACS Catal.*, 2016, **6**, 1345–1353.
74 W.-T. Kim and W.-Y. Choi, *Sens. Actuators, A*, 2017, **260**, 178–184.
75 L. Li, G. Q. Liu, K. Huang, Y. H. Chen, L. X. Gong and F. L. Tang, *Optik*, 2013, **124**, 2519–2521.
76 Y. Long, L. Shen, H. Xu, H. Deng and Y. Li, *Sci. Rep.*, 2016, **6**, 32312.
77 V. A. Tolmachev, E. V. Astrova, J. A. Pilyugina, T. S. Perova, R. A. Moore and J. K. Vij, *Opt. Mater.*, 2005, **27**, 831–835.
78 Y. Lu, H. Yu, S. Chen, X. Quan and H. Zhao, *Environ. Sci. Technol.*, 2012, **46**, 1724–1730.
79 L. Zhang, C.-Y. Lin, V. K. Valev, E. Reisner, U. Steiner and J. J. Baumberg, *Small*, 2014, **10**, 3970–3978.
80 J.-N. Liu, Q. Huang, K.-K. Liu, S. Singamaneni and B. T. Cunningham, *Nano Lett.*, 2017, **17**, 7569–7577.
81 V. G. Kravets, A. V. Kabashin, W. L. Barnes and A. N. Grigorenko, *Chem. Rev.*, 2018, **118**, 5912–5951.
82 H. Benisty and C. Weisbuch, in *Progress in Optics*, ed. E. Wolf, Elsevier, London, 2006, vol. 49, pp. 177–281.
83 Q. Zhou, P. Dong, L. Liu and B. Cheng, *Colloids Surf., A*, 2005, **253**, 169–174.
84 H. Míguez, F. Meseguer, C. López, A. Blanco, L. Vázquez, R. Mayoral, M. Ocaña and L. M. Liz-Marzán, *Adv. Mater.*, 1998, **10**, 480–483.
85 C. Hua, H. Xu, P. Zhang, X. Chen, Y. Lu, Y. Gan, J. Zhao and Y. Li, *Colloid Polym. Sci.*, 2017, **295**, 1655–1662.
86 M. Curti, G. L. Robledo, P. C. dos Santos Claro, J. H. Ubogui and C. B. Mendive, *Mater. Res. Bull.*, 2018, **101**, 12–19.
87 L. Liu, S. K. Karuturi, L. T. Su and A. I. Y. Tok, *Energy Environ. Sci.*, 2011, **4**, 209–215.
88 M. Curti, G. Zvitco, M. A. Grela and C. B. Mendive, *Chem. Phys.*, 2018, **502**, 33–38.
89 M. Wu, J. Liu, J. Jin, C. Wang, S. Huang, Z. Deng, Y. Li and B.-L. Su, *Appl. Catal., B*, 2014, **150–151**, 411–420.
90 T. K. N. Nguyen, F. Grasset, S. Ishii, H. Fudouzi and T. Uchikoshi, *Mater. Adv.*, 2024, **5**, 8615–8628.
91 P. Dai, W. Su, Z. Xian, X. Wei, S. Tang, G. Huang, C. Sun, W. Han, L. Zhu and H. You, *Langmuir*, 2024, **40**, 10936–10946.
92 S. Zeng, E. Vahidzadeh, C. G. VanEssen, P. Kara, R. Kisslinger, A. Goswami, Y. Zhang, N. Mahdi, S. Riddell, A. E. Kobryn, S. Gusarov, P. Kumar and K. Shankar, *Appl. Catal., B*, 2020, **267**, 118644.
93 G. Rosolen and A. Cola, in *Proc. 2006 IEEE Conf. Microwaves, Antennas, Propagation & EMC Technologies for Wireless Communications (IEEE COMMAD)*, IEEE, 2006, pp. 66–69.
94 M. Belotti, M. Galli, D. Bajoni, L. C. Andreani, G. Guizzetti, D. Decanini and Y. Chen, *Microelectron. Eng.*, 2004, **73–74**, 405–411.
95 S. Matsushita, M. Hayashi, T. Isobe and A. Nakajima, *Crystals*, 2012, **2**, 1483–1491.
96 H. Segawa, N. Abrams, T. E. Mallouk, I. Divliansky and T. S. Mayer, *J. Am. Ceram. Soc.*, 2006, **89**, 2473–2478.
97 C. Marichy, N. Muller, L. S. Froufe-Pérez and F. Scheffold, *Sci. Rep.*, 2016, **6**, 21818.
98 J. Peng, Y. Lu, J. Liu, B. Yang and Y. Ding, *Opt. Laser Technol.*, 2023, **160**, 109089.
99 C.-K. Chung and C.-A. Ku, *Annu. Rev. Res.*, 2022, **7**, 001.

100 M. V. Pyatnov, I. R. Volkova, D. S. Buzin, S. Y. Vetrov, M. N. Volochaev, I. I. Ryzhkov and I. V. Timofeev, *JETP Lett.*, 2025, **121**, 166–169.
101 Y. Zhao, B. Yang, J. Xu, Z. Fu, M. Wu and F. Li, *Thin Solid Films*, 2012, **520**, 3515–3522.
102 Y. Wang, D.-B. Xiong, W. Zhang, H. Su, Q. Liu, J. Gu, C. Zhu and D. Zhang, *Catal. Today*, 2016, **274**, 15–21.
103 D. Chaparro and E. Goudeli, *J. Phys. Chem. C*, 2023, **127**, 13389–13397.
104 M. O. A. Erola, A. Philip, T. Ahmed, S. Suvanto and T. T. Pakkanen, *J. Solid State Chem.*, 2015, **230**, 209–217.
105 J. I. L. Chen, E. Loso, N. Ebrahim and G. A. Ozin, *J. Am. Chem. Soc.*, 2008, **130**, 5420–5421.
106 T.-H. T. Le, T.-T. Bui, H. V. Bui, V.-D. Dao and L. L. T. Ngoc, *Catalysts*, 2021, **11**, 761.
107 L. Sanchez-Garcia, C. Tserkezis, M. O. Ramirez, P. Molina, J. J Carvajal, M. Aguilo, F. Diaz, J. Aizpurua and L. E. Bausa, *Opt. Express*, 2016, **24**, 8491–8500.
108 J. Serbin, A. Ovsianikov and B. Chichkov, *Opt. Express*, 2004, **12**, 5221–5228.
109 D. R. Ranasinghe, G. Doerk, B. R. Aryal, C. Pang, R. C. Davis, J. N. Harb and A. T. Woolley, *Nanoscale*, 2023, **15**, 2188–2196.
110 K. Liu, C. Zheng, S. Gao, X. Chen, S. Zhang and T. Cao, *Engineering*, 2025, **49**, 134–140.
111 X. Zhang, Y. Liu, S.-T. Lee, S. Yang and Z. Kang, *Energy Environ. Sci.*, 2014, **7**, 1409–1419.
112 T. K. Rahul and N. Sandhyarani, *Nanoscale*, 2015, **7**, 18259–18270.
113 S. N. Bonvicini and Y. Shi, *ACS Appl. Nano Mater.*, 2022, **5**, 14850–14861.
114 T. L. Madanu, L. Chaabane, S. R. Mouchet, O. Deparis and B.-L. Su, *J. Colloid Interface Sci.*, 2023, **647**, 233–245.
115 C. Wang, X. Guo and X. Wu, *Sci. Rep.*, 2024, **14**, 26169.
116 J. Z. Y. Tan, Y. Fernández, D. Liu, M. Maroto-Valer, J. Bian and X. Zhang, *Chem. Phys. Lett.*, 2012, **531**, 149–154.
117 S. Zhang, B. Peng, S. Yang, H. Wang, H. Yu, Y. Fang and F. Peng, *Int. J. Hydrogen Energy*, 2015, **40**, 303–310.
118 Y. Wu, Q. Liu, T. Liu, J. Wang and S. Xu, *J. Alloys Compd.*, 2022, **910**, 164883.
119 L. Qin, G. Wang and Y. Tan, *Sci. Rep.*, 2018, **8**, 16198.
120 Y. Jiao, C. Wang, D. Zhao, Y. Xu and H. Wang, *Energy Technol.*, 2016, **4**, 956–964.
121 K. H. Leong, H. Y. Chu, S. Ibrahim and P. Saravanan, *Beilstein J. Nanotechnol.*, 2015, **6**, 428–437.
122 F. Scotognella, G. Della Valle, A. R. S. Kandada, M. Zavelani-Rossi, S. Longhi, G. Lanzani and F. Tassone, *Eur. Phys. J. B*, 2013, **86**, 154.
123 Z. Liu, Y. Zhong, I. Shafei, R. Borman, S. Jeong, J. Chen, Y. Losovyj, X. Gao, N. Li, Y. Du, E. Sarnello, T. Li, D. Su, W. Ma and X. Ye, *Nat. Commun.*, 2019, **10**, 1394.
124 M. Ivanchenko, V. Nooshnab, A. F. Myers, N. Large, A. J. Evangelista and H. Jing, *Nano Res.*, 2022, **15**, 1579–1586.
125 G. Collins, A. Lonergan, D. McNulty, C. Glynn, D. Buckley, C. Hu and C. O'Dwyer, *J. Mater. Chem. A*, 2022, **10**, 19538–19555.
126 X. Huang, W. Gu, S. Hu, Y. Hu, L. Zhou, J. Lei, L. Wang, Y. Liu and J. Zhang, *Catal. Sci. Technol.*, 2020, **10**, 3694–3700.
127 P. Babu, H. Park and J. Y. Park, *Surfactant Sci. Technol.*, 2023, **1**, 29.
128 S. Jin, Y.-F. Zhang, X.-J. Du, Q. Huang and Z. Chen, *Environ. Sci.: Nano*, 2023, **10**, 1482–1493.
129 T.-M. Chen, G.-Y. Xu, H. Ren, H. Zhang, Z.-Q. Tian and J.-F. Li, *Nanoscale Adv.*, 2019, **1**, 4522–4528.
130 M. V. Pyatnov, R. G. Bikbaev, I. V. Timofeev, I. I. Ryzhkov, S. Y. Vetrov and V. F. Shabanov, *Photonics*, 2023, **10**, 64.
131 L. Ferrier, H. S. Nguyen, C. Jamois, L. Berguiga, C. Symonds, J. Bellessa and T. Benyattou, *APL Photonics*, 2019, **4**, 106101.
132 S. A. Mahyoub, A. Hezam, F. A. Qaraah, K. Namratha, M. B. Nayan, Q. A. Drmosh, D. Ponnamma and K. Byrappa, *ACS Appl. Energy Mater.*, 2021, **4**, 3544–3554.
133 Z. Zhang, J. Huang, Y. Fang, M. Zhang, K. Liu and B. Dong, *Adv. Mater.*, 2017, **29**, 1606688.
134 C. Yang and Q. Li, *J. Photochem. Photobiol., A*, 2019, **371**, 118–127.
135 Z. Xu, F. Wang, L. Feng and Y. Chen, *Opt. Mater.*, 2023, **139**, 113770.
136 J. Stępnik, A. Kisielewska and I. Piwoński, *Catal. Sci. Technol.*, 2024, **14**, 4274–4287.
137 S. Sarkar, V. Gupta, T. Tsuda, J. Gour, A. Singh, O. Aftenieva, A. M. Steiner, M. Hoffmann, S. Kumar, A. Fery, J. Joseph and T. A. F. Konig, *Adv. Funct. Mater.*, 2021, **31**, 2011099.
138 V. Gupta, S. Sarkar, O. Aftenieva, T. Tsuda, L. Kumar, D. Schletz, J. Schultz, A. Kiriy, A. Fery, N. Vogel and T. A. F. Konig, *Adv. Funct. Mater.*, 2021, **31**, 2105054.
139 J. Liu, H. Zhao, Z. Wang, T. Hannappel, U. I. Kramm, B. J. M. Etzold and Y. Lei, *Sol. RRL*, 2022, **6**, 2200181.
140 A. Tanaka, K. Teramura, S. Hosokawa, H. Kominami and T. Tanaka, *Chem. Sci.*, 2017, **8**, 2574–2580.
141 A. A. Melvin, K. Illath, T. Das, T. Raja, S. Bhattacharyya and C. S. Gopinath, *Nanoscale*, 2015, **7**, 13477–13488.
142 M. Herran, S. Juergensen, M. Kessens, D. Hoeing, A. Koppen, A. Sousa-Castillo, W. J. Parak, H. Lange, S. Reich, F. Schulz and E. Cortes, *Nat. Catal.*, 2023, **6**, 1205–1214.
143 C. Jin, K. Su, L. Tan, X. Liu, Z. Cui, X. Yang, Z. Li, Y. Liang, S. Zhu, K. W. K. Yeung and S. Wu, *Mater. Des.*, 2019, **177**, 107845.
144 Q. Huang, T. D. Canady, R. Gupta, N. Li, S. Singamaneni and B. T. Cunningham, *ACS Photonics*, 2020, **7**, 1994–2001.